The Analysis, Design, Construction and Testing of an Experiment to Study Instabilities in Distributed Parameter Systems of Uncountable Dimension

by

Victor Owuor

S.B. Aero., Massachusetts Institute of Technology (May 1992)
S.B. Elec., Massachusetts Institute of Technology (Feb 1993)

Submitted to the Department of Aeronautics and Astronautics
in partial fulfillment of the requirements for the degree of

Master of Science in Aeronautics and Astronautics

at the

MASSACHUSETTS INSTITUTE OF TECHNOLOGY

May 1994

Author ....
Department of Aeronautics and Astronautics
May 18, 1994

Certified by .....
Prof. James D. Paduano
Assistant Professor, Aeronautics and Astronautics
Thesis Supervisor

Accepted by .....
Prof. Harold Y. Wachman
Chairman, Departmental Graduate Committee

The Analysis, Design, Construction and Testing of an Experiment to Study Instabilities in Distributed Parameter Systems of Uncountable Dimension

by

Victor Owuor

Submitted to the Department of Aeronautics and Astronautics
on May 18, 1994, in partial fulfillment of the
requirements for the degree of
Master of Science in Aeronautics and Astronautics

Abstract

An experiment to study the Kelvin-Helmholtz shear layer instability was designed, constructed and tested. The objective was to extend ideas about controlling infinite dimensional, distributed parameter systems employed at the MIT Gas Turbine Laboratory to systems of uncountable dimension. The experiment showed the uncountable dimensions predicted by the linear model but there were slight deviations due to dissipation of energy (probably by viscosity). As predicted by the linear model of the instability, all frequencies convected downstream in the tunnel at the same rate and a narrow band of them became unstable at high tunnel velocity.

Thesis Supervisor: Prof. James D. Paduano
Title: Assistant Professor, Aeronautics and Astronautics

Acknowledgments

I thank Prof. Paduano for his support, help and encouragement through this project and for his patience in going over this thesis. I am grateful to Harald Weigl for his friendship and words of encouragement at those very dark moments in the lab. This would never have been accomplished if it were not for him. I would also like to thank Don and Earle at the project laboratory who took time to help me with construction even though they did not have to. Thanks go to Victor and Jimmy of the MIT, Gas Turbine Laboratory.

I owe all I have to my parents who struggled to bring us up through very hard times. Any success that I enjoy is yours. Thanks go to my siblings who tolerated me. I miss you all and look forward to my return.

I owe any motivation I have to the boys of 6Sc1A who, even though they had never seen a computer and had only heard of calculators, were determined to make their mark in science. Such ambition is bound to be rewarded with success. FM with VPO is still the best learning environment I have been in.

I would also like to thank all my friends at the frat house who made my stay in college anything but a learning experience. I will miss you and the 'spew sessions'.

Contents

List of Figures

List of Tables

Chapter 1

Introduction

1.1 Motivation and Introduction to Infinite Dimensional Systems

A lot of work has been done on the control of finite dimensional systems. These systems are represented by time-ordinary differential equations. Given a finite number of parameters describing the system (i.e. states), the evolution of the system can be uniquely determined. The number of states needed to describe the system is determined by the number of differential equations and the highest order derivative in each of the equations. There are many texts that describe both classical [Van de Vegte, 90] and also newer optimal control techniques for such systems [Kirk, 70]. the control of finite dimensional systems is so well understood that there are computer packages such as Matlab [Math Works Inc.] that can be used to design controllers with a minimal understanding of the underlying theory. We do not have the same understanding of infinite dimensional systems.

Infinite dimensional systems require an infinite number of parameters describing the state of the system at any one time in order to predict its future. For example, in order to describe the thermal condition in a room, the temperature at every point in the room must be known. This is an infinite dimensional system because there is an infinite number of points in the room if continuum mechanics is assumed. Systems are

normally represented by partial differential equations that involve not only derivatives with respect to time but also partial derivatives with respect to a spatial dimension. As a result, the analysis and understanding of these systems require greater mathematical sophistication than for finite dimensional systems. Almost all prior work in the control of infinite dimensional systems has been theoretical, involving functional analysis and operator theory [Banks] . To date, this work has found little practical application.

[Paduano, 92] is a description of a method for successfully controlling an infinite dimensional instability in a compressor. The states of the compressor are given by the flow rate at different points about the annulus of the compressor. There is both an infinite and uncountable number of points on the annulus and so there appear to be an uncountable infinity of states. However, the flow rate can be represented by a spatial Fourier series taking the position along the annulus as the spatial dimension. Since the annulus is circular, the flow rate is periodic with a period equal to the perimeter of the annulus. This reduces the number of states to the countable infinity of terms in the Fourier series expansion of the flow rate. This Fourier space is a countable orthonormal basis in which the original system can be accurately described.(i.e. It is a way of describing the system using only a countable number of states.) What is more, the flow in the compressor changes smoothly about the annulus so the higher harmonics in the Fourier series are much smaller and can be ignored without significant losses in accuracy (i.e. the high spatial frequency harmonics are natural very stable and are not observed in the system). The order of the model can therefore be reduced by ignoring the higher terms in the Fourier series. The low frequency harmonics in the Fourier series expansion are a finite orthonormal basis that can capture the state of the actual system to an arbitrary accuracy by increasing the number of Fourier harmonics included. As a result, the infinite dimensional system is represented to arbitrary accuracy by a countable number of Fourier harmonics. Traditional control theory design methods applied to this finite dimensional system have been used to control the infinite dimensional system with success.

This approach involving the approximation of the infinite dimensional system by a

finite dimensional one is inevitable if a computer is to be used to control it because the computer only has a finite number of states and cannot represent the actual system let alone implement a control strategy based on it. One is faced with the choice of either doing the analysis and design for the infinite dimensional system and then approximating the resulting control scheme with a finite number of measurements from the system, or building a finite dimensional model of the system based on these measurements and designing a control system based on this model. The second scheme is more promising because it takes advantage of the already existing knowledge and tools for the control of finite dimensional systems.

Although the compressor for which this approach has been implemented [Paduano, 92] has an infinite number of states, they are countable. This is evidenced by their representation by a countable number of terms in a Fourier series. The motivation behind this thesis is to see if the same success can be achieved in systems with an uncountable number of modes. The number of modes in the compressor is countable because the flow rates have to be periodic. The Kelvin-Helmholtz, shear layer instability has no such boundary conditions and cannot be represented by a Fourier series. It therefore has an uncountable infinity of modes. The long term goal of this project is to find a finite dimensional system that can be used to design control scheme for this system. This work is the first step towards this goal. It involves the design and construction of an experiment and the demonstration that it does exhibit the uncountable infinity of dimensions that is required.

1.2 Introduction to the Experiment

[Chandrasekhar, 68] predicts that the shear layer at the boundary between fluids in relative motion becomes unstable above a certain threshold velocity. This instability manifests itself as waves on the boundary of the fluids that travel at the mean velocity of the fluids. Although these waves have been observed in air flowing over water at velocities above this threshold, no effort has ever been made to observe and characterize the system and compare it with the predictions of the linear, non-viscous

model. An experiment was designed in an effort to do this

The experiment consists of a tank containing eugenol (clove oil) that has water flowing over it. An airfoil is used to deflect the boundary between the two fluids and thus excite the instability. A video camera measures the displacements of the fluid boundary, thus sensing the size of the disturbances at a certain sampled points. Input/output measurements were taken in an effort to identify the system behavior and compare it with that predicted by the theory outlined in chapter 3.

Because of the complexity of non-linear analysis of the system, a linear analysis was done and its results used to predict the behavior of the experiment.

The experiment displayed a lot of the traits predicted. All the waves in the shear layer convected at the same group velocity and it was also shown that as the velocity of the flow increased, a certain band of frequencies became increasingly unstable. However, the linear prediction that all other waves would be marginally stable was false. They were stable and got smaller as they traveled along the shear layer.

1.3 Outline

The novelty and complexity of the dynamics of the experiment make its design impossible to understand without some knowledge of the underlying theory. Chapter 2 is a brief overview of the dynamics of the linear model of the shear layer.

Chapter 3 is a description of the experiment and the issues that were considered in its design and construction. This information is especially useful for someone that needs to alter the tunnel or construct a similar one.

Chapter 4 is a description of the airfoil dynamics and how it affects the shear layer. Chapter 5 completes the description of the modeling by explaining the effects of sampling and having a tunnel of finite length on the observed transfer function and also the impact of stabilizing the system over this range on the stability of the entire system.

The results are presented in chapter 5. They are compared with the predictions of the models in chapters 2, 4 and 5 and attempts are made to explain the differences.

Chapter 2

Theoretical Analysis of Undriven System

It is critical that a theoretical analysis of the experimental setup be done so that we know what to expect from the experiment and how to look for it. This theoretical analysis is also necessary to ensure that the experiment will be in the regime over which the system is unstable.

2.1 Variables Describing System

The figure 2-1 shows a schematic of the experimental setup. It comprises two fluids of different densities. The one on top is less dense and is traveling at a velocity U relative to the one below. The velocity of any one liquid is assumed constant through that whole liquid for simplicity of analysis. This assumption is reasonable when the wavelengths considered are big compared to the size of the boundary layer between the two liquids. The linear model, which will be described later in this chapter, predicts that the flow is stable for short wavelengths so the assumption holds for the longer unstable wavelengths we are interested in.

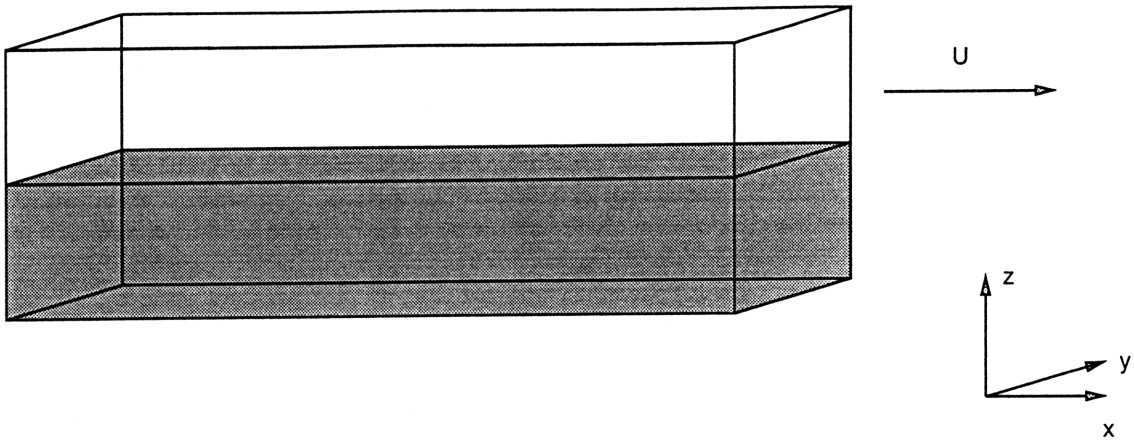

Figure 2-1: Schematic showing definition of independent variables

2.1.1 Independent variables

The independent variables are the coordinate frame in which the problem is described (see figure 2-1)

- x: This is the displacement in the direction of the flow.
- y: This is the displacement in the direction parallel to the interface between the two liquids but normal to the flow.
- z: This is the displacement in direction perpendicular to the interface between the two fluids. It is taken to be zero at the interface and to increase as one moves up.

2.1.2 Dependent variables

These are the variables that describe the state of the system and are in general functions of the independent variables. They are represented as perturbation variables with the mean values being the conditions of the undisturbed system and the perturbations being the small disturbances from this mean value. They are listed below.

- $\rho + \delta\rho$: This is the density of the fluid.

- $P + \delta P$: This is the pressure of the fluid.
- $U + u$: This is the velocity of the fluid in the x direction U is the free stream velocity and u is the local variation of the free stream velocity.
- v is the velocity of the fluid in the y direction.
- w is the velocity of the fluid in the z direction.

2.2 Equations Describing the System

It can be shown [Chandrasekhar, 68] that the system above is described by the set of equations listed below.

- For momentum in the x direction:

$$\rho\frac{\partial u}{\partial t} + \rho U\frac{\partial u}{\partial x} + \rho w\frac{dU}{dz} - \frac{d\mu}{dz}(\frac{\partial w}{\partial x} + \frac{\partial u}{\partial z}) = -\frac{\partial \delta P}{\partial x} \tag{2.1}$$

  The viscosity term of the form $\mu\bigtriangledown^2 u$ that is normally in the momentum equation is zero as we will assume a solution that is of the form:

$$\delta u = \delta u(z)e^{i(k_x x + k_y y + nt)}$$

  for which the divergence squared is zero. It is omitted in the equation above for this reason.

- For momentum in the y direction:

$$\rho\frac{\partial v}{\partial t} + \rho U\frac{\partial v}{\partial x} - \frac{d\mu}{dz}(\frac{\partial w}{\partial y} + \frac{\partial v}{\partial z}) = -\frac{\partial \delta P}{\partial y} \tag{2.2}$$

  The viscosity term of the form $\mu \bigtriangledown^2 v$ is zero for the same reason as described above and is omitted.

- For momentum in the z direction:

$$\rho\frac{\partial w}{\partial t} + \rho U\frac{\partial w}{\partial x} - 2\frac{d\mu}{dz}\frac{\partial w}{\partial z} = -\frac{\partial \delta P}{\partial z} - g\delta\rho + T_s(\frac{\partial^2 \delta z_s}{\partial x^2} + \frac{\partial^2 \delta z_s}{\partial y^2})\delta_d(z - z_s) \quad (2.3)$$

  The last term with T_s is a surface tension term at the surface separating the two liquids. $\delta_d(z - z_s)$is the dirac delta function. It is an impulse of area 1 at z_s and is used in the equation because the surface tension is non-zero only at the surface. Again, viscosity term of the form $\mu \bigtriangledown^2 w$ is omitted.

- The velocity of the fluids will be much lower than the speed of sound and so the fluids will appear incompressible. Since the density of a particle does not change as it moves through the liquid:

$$\frac{\partial \delta\rho}{\partial t} + U\frac{\partial \delta\rho}{\partial x} = -w\frac{d\rho}{dz} \quad (2.4)$$

- The velocity of the boundary between the two liquids is the same as the velocity of the particles of the liquids at the boundary.

$$\frac{\partial \delta z_s}{\partial t} + U_s\frac{\partial \delta z_s}{\partial x} = w(z_s) \quad (2.5)$$

- From the conservation of mass:

$$\frac{\partial u}{\partial x} + \frac{\partial v}{\partial y} + \frac{\partial w}{\partial z} = 0 \quad (2.6)$$

2.3 Solving the Equations

We are interested in wave-like disturbances of the form:

$$\delta q = \delta q(z)e^{i(k_x x + k_y y + nt)}$$

where q is the perturbation variable of interest. Substituting this form for the perturbation variables and writing $\frac{\partial}{\partial z}$ as D in the equations above,

$$(\rho in + \rho U i k_x - (D\mu)D)u + (\rho(DU) - ik_x(D\mu))w = -ik_x\delta P \tag{2.7}$$

$$(\rho in + \rho U i k_x - (D\mu)D)v - ik_y(D\mu)w = -ik_y\delta P \tag{2.8}$$

$$(\rho in + \rho U i k_x - (D\mu)D)w - (D\mu)Dw = -D\delta P - g\delta\rho - (k_x^2 + k_y^2)T_s\delta z_s\delta_d(z - z_s) \tag{2.9}$$

$$i(n + k_xU)\delta\rho = -wD\rho \tag{2.10}$$

$$i(n + k_xU)\delta z_s = w_s \tag{2.11}$$

$$i(k_xu + k_yv) = -Dw \tag{2.12}$$

If equation 2-7 and 2-8 are multiplied by ik_x and ik_y respectively and then added together and equation 2-12 used to eliminate u and v:

$$[\rho in + \rho U i k_x - (D\mu)D]Dw - [i\rho k_x(DU) + (D\mu)k^2]w = -k^2\delta P \tag{2.13}$$

where $k^2 = k_x^2 + k_y^2$.

Substituting $\delta\rho$ from equation 2-10 and δz_s from equation 2-11 in equation 2-9:

$$(\rho in + \rho U i k_x - 2(D\mu)D)w = -D\delta P - ig(D\rho)\frac{w}{n + k_xU} + ik^2\frac{T_sw}{n + k_xU}\delta_d(z - z_s) \tag{2.14}$$

Eliminating δP from equation 2-13 and 2-14,

$$\begin{aligned} D\{[\rho n + \rho U k_x &+ i(D\mu)D]Dw - [\rho k_x(DU) - i(D\mu)k^2]w\} \\ &- k^2(\rho n + \rho U k_x + 2i(D\mu)D)w \\ &= gk^2((D\rho) - \frac{k^2}{g}T_s\delta_d(z - z_s))\frac{w}{n + k_xU} \end{aligned}$$

For the problem that we are interested in, U and ρ and μ are not functions of z so DU, $D\rho$ and $D\mu$ are all zero inside any one of the fluids. The fluid away from the

interface of the two liquids is therefore described by:

$$(k^2 - D^2)(\rho n + \rho U k_x)w = 0 \tag{2.15}$$

The boundary conditions are that the velocity normal to the wall, w, is zero at the wall, $z = \pm d$, and that the velocity of the boundary in the z direction, $\frac{w}{n+k_xU}$, is the same in both liquids. The solution to the equation above that satisfies these conditions is:

$$w_1 = A(n + k_xU_1)(e^{k(d+z)} - e^{-k(d+z)}) \quad z \leq 0 \tag{2.16}$$

$$w_2 = A(n + k_xU_2)(e^{k(d-z)} - e^{-k(d-z)}) \quad z \geq 0 \tag{2.17}$$

Assuming large d relative to $\frac{1}{k}$ these solutions reduce to

$$w_1 = A(n + k_xU_1)e^{kz} \quad z \leq 0 \tag{2.18}$$

$$w_2 = A(n + k_xU_2)e^{-kz} \quad z \geq 0 \tag{2.19}$$

2.3.1 The Fourth Boundary Condition

If equation 2-15 is taken across the boundary of the two liquids, it provides yet another boundary condition that must be satisfied by the two liquids. If it is integrated between $z_s + \epsilon$ and $z_s - \epsilon$ in the limit ϵ tending toward zero,

$$\begin{aligned} \Delta_s\{[\rho n + \rho U k_x + i(D\mu)D]Dw &- [\rho k_x(DU) - i(D\mu)k^2]w\} \\ &= gk^2\Delta_s(\rho)\frac{w}{n + k_xU} - k^4\frac{T_s w}{n + k_xU} \end{aligned}$$

where $\Delta_s(f) = f_{z=z_s+0} - f_{z=z_s-0}$

Substituting for the discontinuities in density and velocity and for D from the solution in previous section,

$$\begin{aligned} \rho_2(n + k_xU_2)(n + k_xU_2) &+ \rho_1(n + k_xU_1)(n + k_xU_1) \\ &= gk(\rho_1 - \rho_2) + k^3T_s \end{aligned}$$

Writing:

- $\alpha_1 = \frac{\rho_1}{\rho_1+\rho_2}$
- $\alpha_2 = \frac{\rho_2}{\rho_1+\rho_2}$

we have,

$$\begin{aligned} n^2 + 2k_x(\alpha_1 U_1 + \alpha_2 U_2)n &+ k_x^2(\alpha_1 U_1^2 + \alpha_2 U_2^2) \\ &- gk(\alpha_1 - \alpha_2) - \frac{k^3 T_s}{\rho_1 + \rho_2} = 0 \end{aligned}$$

The general form of the solution to this equation is:

$$\begin{aligned} n &= -k_x(\alpha_1 U_1 + \alpha_2 U_2) \\ &\pm \sqrt{gk(\alpha_1 - \alpha_2) + \frac{k^3 T_s}{\rho_1 + \rho_2} - k_x^2 \alpha_1 \alpha_2 (U_1 - U_2)^2} \end{aligned}$$

2.4 Unstable Spatial Frequencies

For a spatial frequency k to be unstable, the square root in the equation above must be complex. Writing the solution as $n = -w \pm i\alpha$ the general solution of the initial problem can be written as:

$$w = (w_+ e^{t\alpha} + w_- e^{-t\alpha}) e^{i(k_x x + k_y y - \omega t)} \tag{2.20}$$

where:

- $\omega = k_x(\alpha_1 U_1 + \alpha_2 U_2)$
- $\alpha = \sqrt{k_x^2 \alpha_1 \alpha_2 (U_1 - U_2)^2 - gk(\alpha_1 - \alpha_2) - \frac{k^3 T_s}{\rho_1 + \rho_2}}$
- w_+ and w_- are constants whose magnitudes depend on the initial conditions of the problem.

Since we hope that the only waves excited in the tunnel will be traveling in the $\hat{x}$ direction, k_y will be equal to zero making $k = k_x$ (see equation 2.13). It can be seen

from the equation above that with $k_y = 0$ the disturbances travel through space with a velocity given by:

$$U_w = (\alpha_1 U_1 + \alpha_2 U_2) \tag{2.21}$$

They grow through time at a rate given by :

$$\alpha = \sqrt{k^2 \alpha_1 \alpha_2 (U_1 - U_2)^2 - gk(\alpha_1 - \alpha_2) - \frac{k^3 T_s}{\rho_1 + \rho_2}} \tag{2.22}$$

A spatial frequency given by k corresponds to a temporal frequency of:

$$\omega = k(\alpha_1 U_1 + \alpha_2 U_2) = kU_w \tag{2.23}$$

If the condition for stability (i.e. the real part of α is negative)is rewritten:

$$k^2 \alpha_1 \alpha_2 (U_1 - U_2)^2 < gk(\alpha_1 - \alpha_2) + \frac{k^3 T_s}{\rho_1 + \rho_2} \tag{2.24}$$

The least stable value of k is given by the minimum of the right side of the equation:

$$k_* = \sqrt{\frac{g}{T_s}(\rho_1 - \rho_2)} \tag{2.25}$$

Thus for the system to be stable:

$$(U_1 - U_2)^2 < \frac{2}{\alpha_1 \alpha_2} \sqrt{\frac{Tg(\alpha_1 - \alpha_2)}{\rho_1 - \rho_2}} \tag{2.26}$$

2.5 Spatial evolution of unstable frequencies

From equation 2-20 the solutions to the differential equation are of the general form:

$$w(x, y, t) = Ae^{t\alpha} e^{i(k_x x + k_y y - \omega t)} \tag{2.27}$$

We are only interested in waves that travel in the flow direction since these are the least stable ones so:

$$w(x,t) = Ae^{t\alpha}e^{i(k_x x-\omega t)} \tag{2.28}$$

Writing out the expressions for the vertical displacements of the boundary at two points separated by a distance x_0:

- for one of the points:

$$w(x,t) = Ae^{t\alpha}e^{i(k_x x-\omega t)} \tag{2.29}$$

- for the other point:

$$w(x-x_0,t) = Ae^{t\alpha}e^{i(k_x x-k_x x_0-\omega t)} \tag{2.30}$$

- looking at the expression for the second point at an earlier time, $t - \frac{x_0}{U_w}$, and using equation 2.23

$$w(x-x_0,t-\frac{x_0}{U_w}) = Ae^{(t-\frac{x_0}{U_w})\alpha}e^{i(k_x x_0-\omega t)} \tag{2.31}$$

The final equation in the set of equations above is the same as the first with the exception of the factor $e^{-\frac{x_0}{U_w}}$ From equation 2.29 and 2.31,

$$w(x,t) = e^{\frac{x_0}{U_w}\alpha(\omega)}w(x-x_0,t-\frac{x_0}{U_w}) \tag{2.32}$$

The first exponential term shows that disturbances grow (or decay depending on the sign of α) as they travel downstream. The second term means that points further downstream are a delayed repetition of upstream points. Disturbances convect downstream at a rate that is independent of their frequency.

Chapter 3

Design of the Experiment

This chapter contains a description of the experimental apparatus. Since the actual ideal conditions cannot be achieved, the experiment was designed to come as close to the conditions described in the analysis as possible.

First is an overview of the construction of the experiment followed by the details of the construction of the test section, the actuation and the sensing mechanism. The last part of the chapter is a comparison of the actual experiment with the assumptions in the linear analysis in chapter 2.

3.1 Overview

Figure 3-1 is a schematic of the experimental apparatus. A pump imparts a velocity to the water that flows around in the experiment. This water flows into a large reservoir and into a smooth contraction. The purpose of the contraction is to reduce the size of the boundary layer before going into the test section. A set of honeycomb flow straighteners also reduces the turbulence in the flow. In the test section, the water flows over eugenol (clove oil). The height of the eugenol/water boundary is carefully adjusted using the manometer shown in the figure to ensure that there is as little turbulence as possible at the point of interface. The water flowing over the stationary clove oil creates the shear layer that is needed to create the instability described in chapter 2. All the important things in the experiment occur in the shear

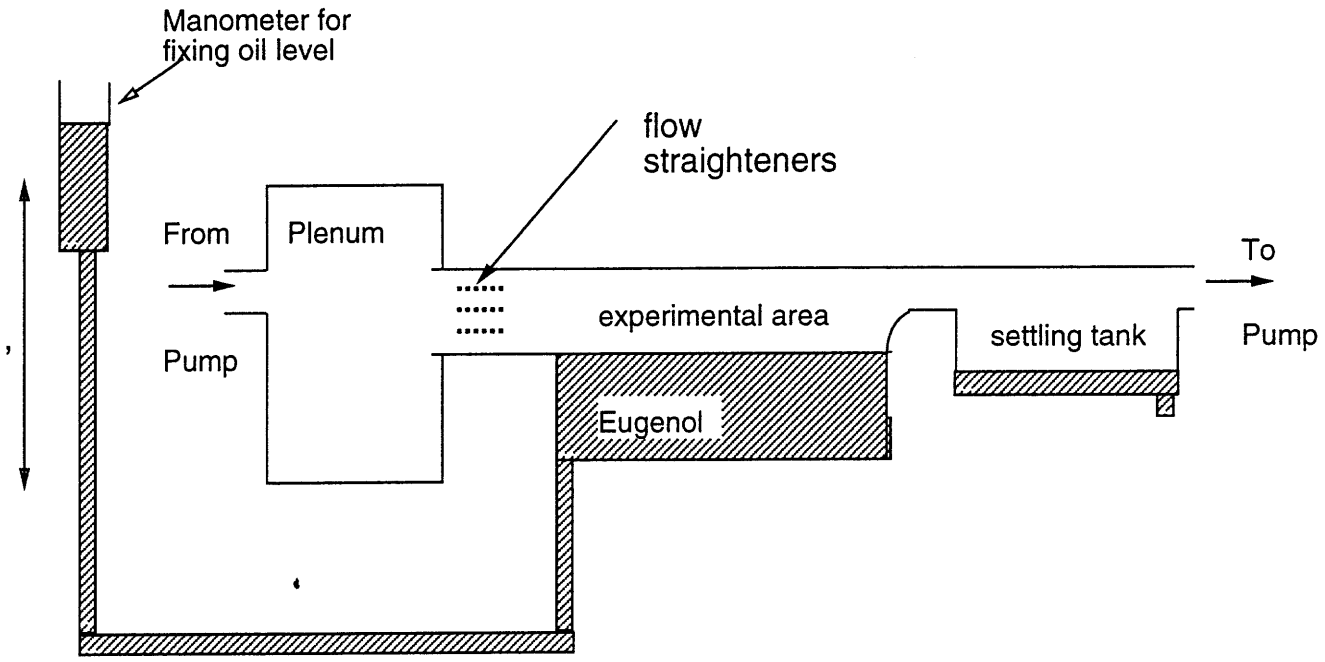

Figure 3-1: Schematic showing overview of experimental setup

layer which will be called the 'experimental area'.

As the water leaves the experimental area, it is important that as little of the eugenol flows out of the test section as is possible. To ensure this, there is a small, smooth step leading into a settling tank, which collects any eugenol that does flow out of the test section. The settling tank has a drain that can be used to recover eugenol that is lost from the test section. The water then circulates back into the pump.

The pump is a centrifugal three phase electrical induction motor pump. The maximum flow rate that it can support is $0.01568 m^3 s^{-1}$.

3.1.1 The Experimental Area

This is the most important part of the experiment. In order for the experiment to work, it is important that:

- the two fluids have a relative velocity that is high enough for them to go unstable. Given the maximum flow rate of the pump, this limits the cross-sectional area of the region the water flows in.

- the tunnel is deep enough that the height of the water and the oil sections appears infinite. This is necessary because it was assumed in equation 2.18 in the analysis.

These are the factors that influenced the dimensioning of the test section.

Equation 2.26 gives the minimum relative velocity of the two liquids for instability. For eugenol and water, the different parameters are as listed below:

- $\rho_2 = \rho_{water} = 10^3 kgm^{-3}$
- $\rho_1 = \rho_{eugenol} = 1.05X10^3 kgm^{-3}$
- $\alpha_2 = \alpha_{water} = \frac{1}{2.05}$ see section 2.3.1.
- $\alpha_1 = \alpha_{eugenol} = \frac{1.05}{2.05}$
- $g = 9.8ms^{-2}$
- $T_s = 0.04Nm^{-1}$

For these parameters, the minimum velocity for instability is given by

$$U > 0.3ms^{-1} \tag{3.1}$$

The tunnel was measured and shown to have a velocity at least twice this. This might seem like a constraint that is satisfied comfortably but viscosity has been ignored in the analysis. Since it is dissipative, its effect will be to further stabilize the tunnel thus increasing the velocity required for instability.

Using Equation 2.25 and the parameters above to get the least stable spatial frequency, we get:

$$k_* = 110m^{-1} \tag{3.2}$$

Using this value of k to get the wavelength $\lambda = \frac{2\pi}{k}$

$$\lambda_* = 1.82\pi cm = 2.36inches \tag{3.3}$$

For the tunnel to be deep enough that the assumption in equation 2.18 (infinite depth) holds, it must be true that $e^{-2\pi\frac{d}{\lambda_*}} << 1$. For the tunnel as designed, the depth of the fluids is 6 inches which makes the left hand side equal to $2X10^{-8}$.

We have verified that for the parameters chosen, this system will go unstable and that the tunnel is deep enough that infinite depth is a reasonable assumption.

3.2 Sensing and Actuation Components

3.2.1 Video Sensing

A video camera is aimed at the fluid boundary in the y direction (see fig 2-1) and is used to sense the deflection of the boundary over a range of positions. A VisionPlus Optical Frame Grabber is used to digitize this picture and download it to a Gateway 486, IBM compatible computer in real time. Programs have been written to find the boundary of the two liquids by finding the point where there is a change in color in the picture captured by the camera [Weigl, 93]. The user can specify the positions in the x direction (see 2-1) that he wants to be tracked in y. The maximum rate at which pictures can be taken per second is 20 Hz ($\frac{2}{3}$ of the 30 Hz sampling rate of the frame grabber). This information is collected real time and could be either stored to aid in system analysis at a later time or used in real time to control the shear layer.

3.2.2 Airfoil Actuation

Different airfoil position command histories are relayed to the airfoil through a Galil Motion Control Board from the computer mentioned in the previous section. The commanded position can be calculated in real-time from the measured displacements of the fluid boundary. The commanded position from the motion control board is used to drive an amplifier which in turn produces the current which drives the motor. The motor has an optical shaft encoder which feeds back the actual position to the Galil board. The Galil board actively controls the position using proportional, integral and derivative feedback. This inner feedback loop was tuned to be fast enough that all the

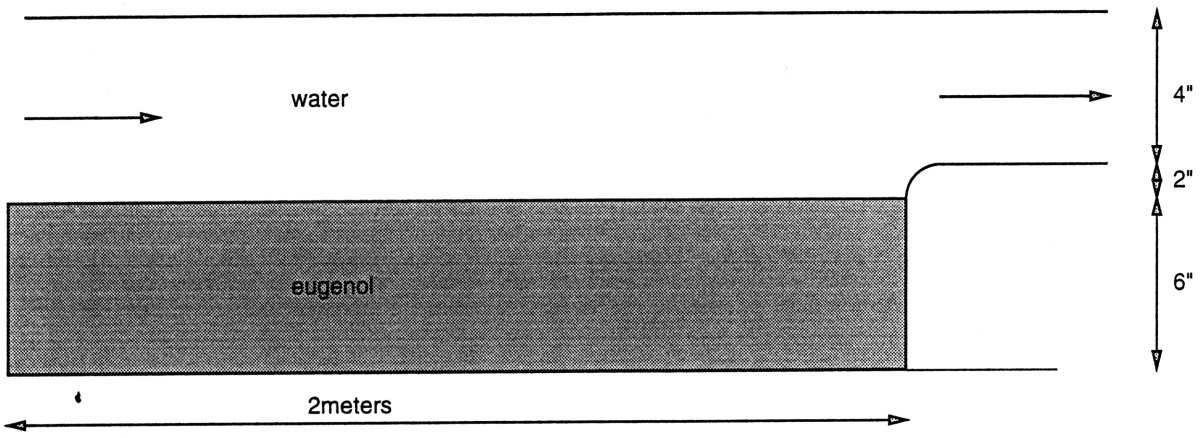

Figure 3-2: Blowup of test section cross-section

dynamics of the motor and its connections to the airfoil can be ignored because the relevant poles and zeros are at frequencies so high that the commanded and actual airfoil position are indistinguishable at the frequencies at which the experiment is run.

3.3 Deviations from Ideal Experiments

Many assumptions were made both in the analysis and also in the design of the test section above. It is important that they are checked to ensure that they are reasonable.

3.3.1 Flow is not Uniform

As a result of the raised edge to the right of figure 3-2, The flow in the experimental area will not be exactly uniform. To ensure that these deviations do not have too large an effect on the experiment, one has to show that the resulting changes in the velocity are small in comparison to the total velocity of the flow.

If the flow of the water above the raised edge is modeled as the top half of a cylinder in a free stream (this is a rough approximation to get the magnitude of

the errors), it can be shown that the resulting errors in the velocity are given by [McCune]:

$$V_x = U(\frac{2a^2z^2}{r^4} - \frac{a^2}{r^2})$$
$$V_z = -U\frac{2a^2xz}{r^4}$$

where:

- U is the velocity of the free stream in which the cylinder is immersed.
- a is the radius of the cylinder. In our case this is taken to be the height of the raised edge above the oil-water boundary. = 2 inches.
- x is the projection of the distance from the center of the cylinder to the point of interest in the direction of the free stream velocity.
- z is the the projection of the this same distance in a direction of normal to that of the stream.
- r is the total distance from the cylinder to the point of interest.

The error in V_x is worst along the boundary of the two liquids ($V_x = U\frac{a^2}{x^2}$). In order for it to be less than a tenth of the free stream velocity, the horizontal distance from the center of the sphere should be at least three times the radius of the sphere. This is only $6inches$ for the experiment. All the data is collected at least 2 feet from the experiment. It is clear that the effect of the step is negligible in the region of interest.

3.3.2 The flow is not two dimensional

Through the analysis we assumed that the flow was 2-dimensional. Derivatives in the y direction (see fig 2-1) were assumed to be zero. The velocities in this direction were also assumed to be zero. This is not true since there are slight variations at the boundary between the fluid and the wall. In order for this assumption to be

reasonable, the width of the boundary layer at the wall should be small in comparison with the total width of the channel. The region covered by the boundary layer must stay much smaller than the width of the tunnel.

If the wall is modeled as a flat plate in a free stream, then the boundary layer width is described by the equation [McCune]:

$$\delta = 5.2\sqrt{\frac{\nu x}{U}} \tag{3.4}$$

where:

- the end of the boundary layer is defined as point at which the velocity of the flow is $.94U$.
- ν is the kinematic viscosity of water $= 1.8X10^{-6}m^2s^{-1}$
- length of tunnel $= x = 1m$
- velocity of tunnel $= U = 0.5ms{-}1$

Using these values, the thickness of the boundary layer at the end of the test section is given by: $1cm = 0.4inches$. The tunnel is $6inches$ wide so the boundary layer is small compared to the width of the tunnel.

Chapter 4

Theoretical Analysis of System with Airfoils

Control of the Kelvin-Helmholtz system was effected using quasi-2-dimensional airfoils. It turns out that if the airfoils are displaced from the fluid boundary by a distance h, more 'states' exist in the system, as a result of the vortex sheet that trails each airfoil. Section 4.1 through 4.4 describe the case where the airfoils are above the shear layer. In section 4.5, we briefly analyze a different form of actuation. In both cases, one or more airfoils is used to excite the shear layer. The rest of the chapter discusses the controllability and observability of the system.

Throughout this analysis, it will be assumed that the changes in the angle of attack are not only small enough that the flow around the airfoils does not separate, but are also small enough that a linear analysis is valid. Special effort was made over the course of the experiment to ensure that the angle of the airfoil was smaller than 30 degrees. The bulk of this section is drawn from previous work [McCune, 88].

4.1 Modeling the flow as a function of a point circulation

For an airfoil at a constant angle of attack, before separation, the circulation around the airfoil is simply proportional to the angle of attack.

$$\Gamma(t) = k\theta$$

This is not true for an airfoil in unsteady flow because there is a wake behind the airfoil which changes the flow around it. This make the relationship dynamic.

The effect of the airfoil on the ambient flow is complicated by the fact that the angle of the attack is constantly being changed in order to control the shear layer. These changes invalidate a steady state flow assumption and unsteady airfoil theory is needed to analyze the situation. We will model the airfoil as a point vortex with circulation Γ in a free stream and then worry about how the vorticity changes with the angle of attack of the airfoil later.

In other words:

$$\Gamma = \Gamma(\theta(t))$$

we will start by assuming:

$$\Gamma = \Gamma(t)$$

and determine the functionality with θ presently.

Circulation is conserved in a flow. The changes in circulation of the airfoil must result in the shedding of an equal and opposite amount of vorticity to conserve the total amount of circulation of the flow. This shed vorticity travels downstream with the velocity of the free stream. If changes in the angle of attack are continuous, then there is a vortex sheet shed behind the airfoil whose intensity depends on the time history of the changes in the circulation about the airfoil. If x is the distance downstream of the airfoil and t is time, the intensity γ of this vortex sheet at a

position, x, and a time, t, is given by:

$$\gamma(x,t) = \frac{-1}{U}\frac{d}{dt}\Gamma(t - \frac{x}{U}) \tag{4.1}$$

where U is the free stream velocity.

We will assume, for simplicity, that the point vortex and its accompanying vortex sheet capture the essential physics of the airfoil. This assumption is true for a narrow airfoil at small angles of attack at distances from the airfoil that are large in comparison to its chord length.

4.2 Modeling the effect of the airfoil on the fluid boundary

Our sole concern is the vertical displacement of the boundary of the two liquids. It turns out that the analysis is much easier if we look only at the vertical velocities of fluid particles at this boundary.

The airfoil is a distance, h, above the fluid boundary. Its effect on the vertical velocity, w, of particles on the boundary of the two liquids can be shown by the Biot-Savart law to be:

$$w(x,t) = -\frac{\Gamma x}{2\pi(x^2+h^2)} - \frac{1}{2\pi}\int_0^\infty \frac{\gamma(\hat{x},t)(x-\hat{x})}{(x-\hat{x})^2+h^2}d\hat{x} \tag{4.2}$$

The first part follows from the distribution of velocities around a point vortex at a point displaced from it. The second part is just the effect of incremental volumes of the vortex sheet integrated over the whole vortex sheet.

4.3 Interaction of the effect of the airfoil with the shear layer

Since the system is linear, the vertical velocity at any point is the sum of that due to the Kelvin-Helmholtz dynamics described in the previous chapter and that due to the airfoil. Writing out this sum, the system is described by:

$$w(x,t) = e^{\alpha\frac{x_0}{U_w}} w(x - x_0, t - \frac{x_0}{U_w}) - \frac{\Gamma x}{2\pi(x^2+h^2)} - \frac{1}{2\pi}\int_0^\infty \frac{\gamma(\hat{x},t)(x-\hat{x})}{(x-\hat{x})^2+h^2} d\hat{x} \quad (4.3)$$

The vortex sheet γ is given by equation 4.1.

4.4 Unsteady Wing Theory and Circulation

Now we will introduce a relationship for how the circulation changes with angle of attack.

Through this analysis, it will be assumed that the changes in the angle of attack are not only small enough that the flow around the airfoil does not separate, but are also small enough that a linear analysis is valid.

For an airfoil at a constant angle of attack, before separation, the circulation around the airfoil is simply proportional to the angle of attack.

$$\Gamma_0(t) = -\pi U_\infty c\theta(t) \quad (4.4)$$

where:

- U_∞ is the free stream velocity.
- c is the chord length of the airfoil

This is not true for an airfoil in unsteady flow because there is a wake behind the airfoil, which changes the flow around it. In the analysis we will take horizontal distance x to be zero at the downstream end of the airfoil. The following classical argument serves to motivate the model:

- The wake changes the direction of the mean flow around the airfoil thus changing the effective angle of attack of the airfoil in the free stream. It can be shown [McCune, 88] by integrating the resulting vertical velocities due to the vortex sheet at the half chord point that this effect is given by [McCune, 88]:

$$\Gamma_1(t) = \frac{c}{2}\int_0^\infty \frac{\gamma(x,t)}{x}dx \tag{4.5}$$

- The vertical velocity resulting from the wake is not zero along the chord of the airfoil. What is more, it is greater on parts of the airfoil further downstream than those upstream. In order to ensure that there is no flow through the airfoil (boundary condition for a hard surface), more circulation is produced by the airfoil. It can be shown [McCune, 88] by integrating these differences in velocities along the airfoil that the circulation produced is:

$$\Gamma_2(t) = \int_0^\infty \gamma(x,t)(\sqrt{\frac{x+c}{x}} - 1)dx \tag{4.6}$$

The three contributions to Γ in equations 4.5, 4.6 and 4.7 can be added to each other as the system is linear to give:

$$\Gamma(t) = -\pi U_\infty c\theta(t) + \frac{c}{2}\int_0^\infty \frac{\gamma(x,t)}{x}dx + \int_0^\infty \gamma(x,t)(\sqrt{\frac{x+c}{x}} - 1)dx \tag{4.7}$$

This equation with equations 4.3 and 4.1 above are the complete formulation of the problem. The objective is to find a time history of the angle of attack θ that stabilizes the system and also minimizes the effects of disturbances on it.

4.5 Analysis for airfoil at boundary between two liquids

As shown in the previous section, vorticity shed from the airfoil further complicates the problem. This trailing vorticity is infinite dimensional and cannot be measured

directly. The unmeasurable states resulting from this vorticity make the controller needed to stabilize the system more complicated. Because of this, it has been suggested that an actuation scheme be found that directly changes the position of the fluid boundary.

If the airfoil were placed at the boundary between the two liquids, we hypothesize that it would not be possible to actuate the flow by changing its angle of attack because:

- when the angle of attack is positive, the trailing edge of the airfoil is inside the stationary fluid, since it just dips into the lower liquid. As a result, there is no change in the exit velocity of the wing and very little actuation occurs. The airfoil does not satisfy the Kutta condition.

- when the angle of attack is negative, the trailing edge rises into the fluid above the boundary. The flow that must expand around the airfoil has a very small velocity and thus separates.

A better way to do the actuation is to have a wing whose camber can be actuated in real time. This approach would attempt to change the exit angle of the flow without changing the height of the trailing edge of the airfoil. This eliminates the potential problem of the airfoil dipping into the static liquid. The result is, strictly speaking, not an airfoil anymore as it is not in a uniform flow. Rather, it is boundary condition on the vertical velocity of fluid elements at the point where the two liquids first meet.

It is hypothesized that the exit angle of the actuator would set the the slope of the shear layer at the exit point when the problem is in steady state. From equation 2.32, the slope of the eigenvalue associated with the mode at a temporal frequency ω is related to the mode by the equation:

$$\frac{d}{dx}w(x,t) = [\alpha(\omega) - i\frac{U}{w}]w(x,t) \tag{4.8}$$

We can therefore find the effect of changing the angle of the shear layer at one point by separating its effect on the different modes and then seeing how each of these

modes evolves. This gives:

$$w_{actuator}(x,t) = \int_0^\infty e^{\alpha(\omega)\frac{x}{U}} e^{i\omega(\frac{x}{U}-t)} \left(\frac{1}{\alpha(\omega) - i\frac{U}{w}} \int_0^\infty \theta_{exit}(\hat{t}) e^{-i\omega\hat{t}} d\hat{t} \right) d\omega \qquad (4.9)$$

The inner integral separates the effect of the slope, $\theta_{exit}(t)$ into its effect on the slopes of the different modes. The fraction that multiplies this integral then converts the effect on the slope into the effect on the entire mode using equation 4.8. The two exponents in the outer integral show the homogeneous evolution of the mode. the outer integral sums the effect over all the modes of the system.

The expression for the entire system is then given by:

$$w(x,t) = e^{\alpha\frac{x_0}{U_w}} w(x - x_0, t - \frac{x_0}{U_w}) + \int_0^\infty e^{\alpha(\omega)\frac{x}{U}} e^{i\omega(\frac{x}{U}-t)} \frac{1}{\alpha(\omega) - i\frac{U}{w}} \int_0^\infty \theta_{exit}(\hat{t}) e^{-i\omega\hat{t}} d\hat{t} d\omega \qquad (4.10)$$

This system is described by only one partial differential equation and has fewer states than the previous one. More importantly, all the variables in the equation ($w(x,t)$ and α_{exit}) are measurable. In the previous description, the magnitude of the vortex sheet trailing the airfoil is not measurable. This system is therefore easier to control since all states are measurable. However, all the effect of the controller occurs downstream of the actuation point so one could never take the limit of the control process as the spatial range tended towards $(-\infty, \infty)$.

4.6 Observability

It is important to keep in mind that the objective of the experiment is to minimize the deflections of the shear layer. Since the deflection of the shear layer over the range of points of concern is measured, all the states relevant to their time evolution must clearly be observable. Unobservable states can be removed by reducing the order of the model without any loss in accuracy of prediction of the evolution of the shear layer. If, for instance, some states of the vortex sheet were unobservable from the shear layer, the model describing the shear layer dynamics would be unchanged by

their removal. By this argument, all the relevant states are observable.

4.7 Controllability

This is the issue that is of greatest concern. If there are eigenmodes whose time evolution cannot be changed using airfoils then the system will not be controllable. This section is an attempt to do a controllability analysis of the problem.

From equations 2.32 and 2.29, the eigenmodes are of the form:

$$w_e(x,t) = e^{-j\omega t}[e^{\frac{\alpha(\omega)}{U_\infty}x}e^{\frac{j\omega}{U_\infty}x}] \tag{4.11}$$

Because of the convection of the shear layer, their is a link between temporal oscillations and the shape of the mode associated with them. Thus the bracketed term gives the shape of the eigenmodes excited by oscillating the airfoil at a frequency ω. Our objective is to quantify the effect of oscillations of the airfoil at this frequency on the mode.

From equation 4.2, the effect of the airfoil can be separated into two components: that due to bound vorticity and that resulting from the vortex sheet that trails it. For simplicity, we will treat the controllability resulting from these two factors separately. This makes sense because the system is linear and so the net effect is the sum of the effect of these two terms.

4.7.1 Controllability From Vortex Sheet

For the low frequencies with which we are concerned, the effect of the vortex sheet is outweighed by that of the bound vorticity for points close to the airfoil. The vortex sheet is therefore only important far away from the airfoil. Because of this, we will assume that in this region, the shear and vortex sheets extend to infinity both in the upstream and downstream directions.

It was shown at the beginning of this section that in order to excite the mode whose shape is given by $e^{\frac{\alpha(\omega)}{U_\infty}x}e^{\frac{j\omega}{U_\infty}x}$ the airfoil must oscillate at the frequency $e^{j\omega t}$.

Since the vortex sheet is a convecting, linear time-invariant function of the oscillations of the airfoil, it will be described by the function:

$$\gamma = \gamma_0 e^{-j\omega t} e^{\frac{j\omega}{2U_w}x} \tag{4.12}$$

There is a factor of (approximately) two in the velocity term because it convects at twice the velocity of the shear layer. From the third term in equation 4.3, the resulting effect on the shear layer is given by the convolution below:

$$w_{vortex}(x,t) = \gamma_0 e^{j\omega t}[e^{\frac{j\omega}{2U_w}x} * \frac{x}{x^2+h^2}] = F_x^{-1}[\delta(w_x - \frac{w}{2U_w})F_x(\frac{x}{x^2+h^2})] \tag{4.13}$$

With $F_x(.)$ being the fourier transform with respect to x. Since convolution is a linear time invariant process, the result is simply the product of the exponent being convolved and a constant whose value is the Fourier transform of the other term evaluated at the frequency of the exponent i.e

$$w_{vortex}(x,t) = Ae^{j\omega t}e^{\frac{j\omega}{2U}x} \tag{4.14}$$

Where A is $F_x(\frac{x}{x^2+h^2})$ evaluated at $w_x = \frac{w}{2U}$.

The issue under investigation when talking about controllability, from equation 4.3, is how much of the eigenmode can be reduced by the addition of this term. If this term is orthogonal to the eigenmode then the eigenmode is not controllable. The two functions under consideration are: $e^{\frac{j\omega}{2U}x}$ and $e^{\frac{\alpha(\omega)}{U}x}e^{\frac{j\omega}{U}x}$. For the case where the eigenmode is neutrally stable, these are harmonics at two different frequencies and are therefore orthogonal. Neutrally stable modes are therefore uncontrollable from the vortex sheet. The vortex sheet can only increase the size of these modes because the magnitude of the sum of the mode and the vortex sheet effect is always greater than the magnitude of the mode (This is a direct result of orthogonality). The same temporal frequency results in different spatial frequencies in the vortex sheet and the shear layer. Since these spatial frequencies are orthogonal, the vortex sheet cannot be used to control the shear layer. The two are either orthogonal in time or in space.

Controllability increases as the flow becomes more unstable and the functions less orthogonal. However, it still remains small. This means that large amplitudes in the vortex sheet are needed to affect shear layer. The inner product of the resulting vortex sheet shape and the eigenmode shape gives a measure of the controllability. It is given by the integral below:

$$\int_0^{\frac{4U\pi}{\omega}} e^{\frac{j\omega}{2U}x} e^{\frac{\alpha(\omega)}{U}x} e^{\frac{j\omega}{U}x} dx = \frac{2U}{2\alpha + 3j\omega}[e^{\frac{4\pi\alpha(\omega)}{\omega}} - 1] \tag{4.15}$$

For small values of alpha, this is simply:

$$\frac{2U}{3j\omega^2} 4\pi\alpha(\omega) \tag{4.16}$$

In order for the mean amplitude of the eigenmode to be reducible, the amplitude must be non-zero. The larger this value relative to the size of the eigenmode, the greater the controllability. The size of the eigenmode is given by:

$$\sqrt{\int_0^{\frac{4U\pi}{\omega}} e^{\frac{\alpha(\omega)+j\omega}{2U}x} e^{\frac{\alpha(\omega)+j\omega}{2U}x} dx} = \sqrt{\frac{U}{2\alpha + 2j\omega}[e^{\frac{8\pi\alpha(\omega)}{\omega}} - 1]} \tag{4.17}$$

For small values of alpha, this gives:

$$\sqrt{\frac{U}{2j\omega^2} 8\pi\alpha(\omega)} \tag{4.18}$$

Since we expect the values of α in the experiment to remain small, the exponents in the expressions above can be linearized to give the ratio of the inner product to the size of the eigenmode as:

$$\frac{8U\pi\alpha(\omega)}{3\omega^2}) / \sqrt{\frac{8U\pi\alpha(\omega)}{2\omega^2}} \tag{4.19}$$

This gives:

$$\frac{3}{\sqrt{2}\omega} \sqrt{8U\pi\alpha(\omega)} \tag{4.20}$$

For these small α, the controllability increases with the speed of the tunnel and with

α. Higher frequencies are harder to control.

4.7.2 Controllability from bound vorticity

From equation 4.3 and the analysis above, the controllability from the bound vorticity is zero if $\frac{x}{x^2+h^2}$ and $e^{\frac{\alpha(\omega)}{U}x}e^{\frac{j\omega}{U}x}$ are orthogonal. The controllability can be measured by the inner product of these functions. The integral for calculating this orthogonality is simply the Laplace transform of $\frac{x}{x^2+h^2}$ evaluated at $s_x = \frac{1}{U}(\alpha(\omega) - j\omega)$. i.e

$$\int_0^\infty \frac{x}{x^2+h^2} e^{-\frac{\alpha(\omega)}{U}x + \frac{j\omega}{U}x} dx \tag{4.21}$$

This can be looked up in any table of Laplace transforms and is not zero at any point. Thus all modes are controllable from the bound vorticity.[Roberts and Sanders] gives the value of the Laplace transform and the result of the substitution gives:

$$-cos(\frac{h}{U}(\alpha(\omega) - j\omega)) \int_{\frac{h}{U}(\alpha(\omega)-j\omega)}^\infty \frac{cosu}{u} du - sin(\frac{h}{U}(\alpha(\omega) - j\omega)) \int_{\frac{h}{U}(\alpha(\omega)-j\omega)}^\infty \frac{sinu}{u} du \tag{4.22}$$

4.7.3 Controllability Conclusion

From the analysis above, it is clear that the vortex sheet has the added peril that excitation of frequencies that are neutrally stable will increase the magnitude of the shear layer displacements. The added states of the shear layer come at a high cost in analysis, design and implementation with little advantage in controllability. It is for this reason that the alternative actuation method described in 4.5 was considered.

Chapter 5

Model Reduction: The Sampled Bounded Range Problem

As explained in the introduction, the objective is find a suitable finite dimensional model of the system described in chapter 2. This section describes the finite dimensional approximation and evaluates how good an estimate of the actual system it is.

The problem is doubly bounded.

- Because the tunnel is bounded, the waves in it do not extend to infinity. We must ensure that this does not affect that tunnel and that any effects of the boundaries of the tunnel are small over the region of concern.
- The Camera only records images of a small portion of the tunnel. The relationship of this observed transfer function to the actual transfer function in the tunnel must be known if we are to identify the parameters ($\alpha(\omega)$ and U) that describe the system (see equation 2.32).

We will characterize the effects of these two bounds. First we will discuss the fact that the tunnel is bounded and then we will go on to discuss the fact that we are only observing a small subset of the shear layer.

5.1 The effect of the bounded tunnel

5.1.1 The vortex sheet

The circulation on the vortex sheet represents the states of the actuator. We assume in the model that it extend an infinite distance downstream. Because the wavelengths are of the order of 3 inches and the tunnel extends at least 60 inches, this is a valid assumption. This shed vorticity is bound to the fluid and flows out of the tunnel and there is no reflection. What is more, the effect of points on the vortex sheet decays as the reciprocal of the square of their distance from the test section. We can therefore approximate the vortex sheet with a sheet of finite length so long as the area over which we observe the tunnel is bounded.

In constructing a discrete model of the vortex sheet, it will be approximated a by a countable number of states obtained by sampling the continuous sheet. By the Nyquist sampling theory, this is valid so long as the spatial sampling frequency is greater than twice the spatial frequency . The bandwidth of the controller is bounded and temporal and spatial wavelengths are related linearly (a direct consequence of convection) so the the spatial frequencies are also band limited. If the sampling rate of the vortex sheet is chosen correctly, a finite model can capture its dynamics.

5.1.2 The shear layer

The geometry of the test rig suggests (and it was observed in experiments) that the disturbances are small at the point where the two fluids first come into contact. The waves have zero amplitude upstream of this point. This is in keeping with the representation of the system given by equation 2.32. The waves grow as they travel downstream but the amplitude at any one point does not increase with time. The instability manifests itself in the spatial dimension because the disturbances travel as time increases. Thus the upstream bound of the tunnel is represented by the model.

The downstream bound of the tunnel is a little more complicated. From figure 3-2, the waves cannot flow in the x direction in the eugenol at the downstream end

of the tunnel because of the barrier. Since the solutions of the shear layer instability (equation 2.32) do not allow waves to travel upstream, this boundary condition must be satisfied by a solution to Laplace's equation (i.e. the homogeneous solution to Laplace's equation). This solution will be of the form:

$$w_0(x,t) = Ae^{ik_x z}e^{k_x(x-x_{boundary})} \tag{5.1}$$

This solution was found by picking the solution of Laplace's equation that does not give rise to waves traveling upstream (no oscillation in the x direction) and decreases as one moves away from the wall (potentials for Laplace's equation are greatest at the boundary). This solution to Laplace's equation decays to $3.4873x10^{-}06$ of its value at the boundary two wavelengths away from the wall. This is only 6 inches from the boundary in our experiment. This effect is negligible in the region of interest.

The fact that the actual tunnel is bounded makes no significant difference to the dynamics of the waves over the region of interest.

5.2 Effect of bounded and sampled camera range

Because the camera only gets information over a small portion of the experiment and this portion is sampled by a computer, the system observed is not the same as the actual system. Unlike the bounds discussed in the previous section, this does not affect the actual dynamics. The measured dynamics are different from the actual ones because of incomplete measurement. Issues of observability and bounds of the errors in estimating the transfer function have to be made for the system to be controlled effectively.

5.2.1 The effect of bounding the range

In the problem as stated in chapter 2, it is assumed that the two liquids extend infinitely both in the positive and negative horizontal directions. It was shown in section 5.1 that the tunnel behaves almost as if it were infinite. However, the camera only

takes information about a small length of this tunnel. The effect of this 'windowing' of the tunnel is explained in this section.

The transfer function from an actuator to the displacement of the boundary or from one point of the boundary to others further downstream is a function of position. It can therefore be written as:

$$w(x,s) = G(x,s)u(s) \tag{5.2}$$

The transfer function that shows the effect of the control on the different spatial harmonics in the displacement of the boundary layer or the evolution of different initial states of the system with time can be found by taking the Fourier transforms of both sides of the equation above to give:

$$\hat{w}(k,s) = \hat{G}(k,s)u(s) \tag{5.3}$$

This transfer function is the system transfer function since it tells how the different spatial eigenfunctions of the system evolve with time. It is this second transfer function that we are interested in. We would like to see how it is changed by looking at the system over a bounded range.

By looking at a finite segment of the tank, we have 'windowed' the displacement of the boundary along the x direction. One way to represent this fact is to assume that it is zero everywhere else but in the region of concern. This is equivalent to windowing the transfer function above i.e.

$$G_m(x,s) = G(x,s)f(x)$$

where:

- $G_m(x,s)$ is the transfer function of the model with the finite range.
- $f(x)$ is a function whose value is one for x within the region of concern and zero elsewhere.

We would like to find out what the effect of this is on the transfer function $\hat{G}(k,s)$.

From Fourier theory, the Fourier transform of a product of two functions is the same as the convolution of the Fourier transforms of the two functions. The effect of windowing on the frequency transfer function is thus a convolution with the sinc function.

$$\hat{G}_m(k,s) = \int_{\infty}^{-\infty} \hat{G}(k-\hat{k},s)\frac{sin(\hat{k})}{\hat{k}}d\hat{k}$$

where:

- $\hat{G}_m(k,s)$ is the transfer function of the model.
- $\frac{sin(k)}{k}$ is the Fourier transform of the boxcar window above.

We now know how the transfer function is changed. It is important to notice that in the limit where the window is very wide, the sinc function looks like an impulse at the origin. In this case, the transfer function is unchanged by windowing.

$$\lim_{x_w \to \infty} \hat{G}_m(k,s) = \hat{G}(k,s) \tag{5.4}$$

The convergence properties in this integral are given by those of the sinc function to an impulse. Since this converges only pointwise, the convergence of the transfer functions is also only pointwise. However, the effect of bounding the range can be made arbitrarily small by increasing the range.

The value at any one spatial frequency in the model will be an average of other frequencies weighted by the sinc function. Because waves travel downstream at a fixed velocity, the spatial frequency $k-\hat{k}$ is associated with the corresponding temporal frequencies by the relation $U_w(\omega-\hat{\omega})$ where U_w is the convection velocity. The convolution can be written as a convolution of temporal frequencies. As a result, the temporal Fourier transform in the expression $G_m(x,jw)$ is also convolved with the sinc function. $G(x,t)$ for the unbounded problem was calculated in chapter 2 (see equation 2.32).

The convolution above will not make the model appear unstable if the actual system is stable since it can be viewed as the response of a stable system to a bounded

input, since convolution is the same as a linear response(i.e. we can view the sinc function as the input to the transfer function.) However the converse is not true. If the actual system has an unstable mode that is not observable under the windowing, the model may appear to be stable even though the actual system is not.

This discussion leads us to the following conclusions concerning windowed observation of the infinite space system:

- Although the measured dynamics are altered by the windowing process, the effects are predictable and the relatively benign. Stable systems appear stable. Unstable eigenmodes may appear stable as a result of the convolution.

- This windowing in the spatial domain has the same effect on the transfer function as time domain windowing since position and time are related by the convection velocity. Thus the properties of the observed system can be tailored by picking a better window than the boxcar. For instance if ringing is undesirable, a Hanning window could be used instead of a boxcar.

- The effect of windowing reduces as the length of the window is increased. If the camera takes information over a long segment, the observed transfer function will be approximately that of the infinite segment.

5.2.2 The effect of sampling

The states of the uncontrolled system are given by the displacements of the shear layer within the range. Thus each point within the region of interest is a state. Since there are an uncountable infinity of points within any finite range, these states are more than one can fit into a computer and so digital control would not be possible. The limitation is not just because the computer has finite memory but also because the memory of the computer is discrete in nature and so even if you had a computer with infinite memory, the memory would still be countable and you would not be able to represent the states of the system. It is therefore imperative that the range be reduced by sampling to yield a new set of states that is at most countable.

From Nyquist sampling theory, spatial frequencies less than half the spatial sampling rate are unchanged by sampling $G(x, jw)$. However, spatial frequencies above this are 'aliased' to lower frequencies in the model ($k_m = mod(k_x, \frac{k_s}{2})$ where k_s is the spatial sampling frequency). Since the velocity of the wave is given by $\frac{\omega}{k}$, aliased waves will appear to travel faster in the model. Simulations show that this causes attenuation of aliased frequencies. The corresponding phase also stops being linear with distance downstream for these temporal frequencies.

As the sampling rate is increased, the range of frequencies that is not aliased is also increased. For an infinite sampling rate, no frequencies are aliased and the model looks like the actual system.

$$\lim_{x_w \to \infty} \hat{G}_m(k, s) = \hat{G}(k, s) \tag{5.5}$$

Convergence is only pointwise since so long as the sampling rate is finite, there are frequencies that are aliased.

Since the system has a maximum spatial wavelength that is unstable, a low pass filter can be used to exclude higher frequencies to avoid this aliasing. The spatial frequencies are proportional to temporal frequencies, so this can be done in time domain. This filtering is accomplished by the low pass filter that is used to avoid temporal aliasing before temporal sampling of the signals for input into the computer. The net result is that the control will not affect high frequencies. This is okay since they are stable anyway.

5.3 Conclusion of model discussion

Based on the previous discussion and on a computer model constructed, we hypothesize that the finite dimensional model captures the essential dynamics of the infinite dimensional problem. What is more, as the order of the finite dimensional model is increased, it converges on the real system. Thus, if we can control the model, then conceptually it would possible to control the real system if one had an infinitely long

shear layer and a computer that could handle a countable infinity of states. Given the nature of the shear layer, more can be said about the accuracy of the model.

If the model appears stable, then it must be the case that the unstable modes are unobservable in the region of interest and are therefore not important. They are unobservable either because they do not show in the tunnel or occur at frequencies higher than the sampling rate. Experimental results (chapter 6) indicate that high frequencies are so stable that attempts to excite them are unsuccessful. Thus a bounded finite dimensional model for this infinite dimensional system should capture the dynamics and converge on the system. The modes in this system are unobservable either because they are lost in the sampling or in the windowing. From the nature of the eigenfunctions (equation 2.31), a mode cannot be lost in the windowing.

Modes lost in the sampling must have a spatial frequency much higher than the sampling rate. These high spatial frequencies result in high viscosity which dissipates them and thus stabilizes them.

5.4 The New Reduced Model

In this finite state model, the linear equations describing the system dynamics (equations 4.3, 4.4 and 4.8) are simply matrix equations. The matrices can be obtained by assuming that the function remains constant over spatial intervals of a length given by the spatial sampling frequency. i.e

$$w(x,t) = w(x_1,t) \quad x_1 \leq x < x_1 + x_s \tag{5.6}$$

with x_s being the spacing between spatial sample positions. After this discretization in space, the convolutions become matrix equations and multiplications are vector multiplications.

They can be written as:

- for equation 4.7,

$$\Gamma(t) = k\theta(t) + \mathbf{T}\vec{\gamma}(t) \tag{5.7}$$

where k is given by $-\pi U_\infty c$ and the matrix $\mathbf{T}$ represents the discretization of the integrals in the original equation.

- for equation 4.1, the solution is not that straight forward. One needs to use the fact that vortex sheet is traveling with the free stream velocity and so it must satisfy the wave equation,

$$\frac{\delta}{\delta t}\gamma(x,t) = -U\frac{\delta}{\delta x}\gamma(x,t) \tag{5.8}$$

everywhere except at $x = 0$. The boundary condition at $x = 0$ is obvious from equation 4.1 and is written below.

$$\gamma(0,t) = -\frac{1}{U}\frac{d}{dt}\Gamma(t) \tag{5.9}$$

The derivatives are linear transformations and can be represented by difference equation matrices in the reduced model. This yields the matrix equation,

$$\dot{\vec{\gamma}} = \mathbf{A}_\gamma\vec{\gamma} + \vec{a}\frac{d^2}{dt^2}\Gamma \tag{5.10}$$

where $\vec{a}$ results from the difference equation at the boundary, $x = 0$. Eliminating Γ using 4.7, this can be reduced to:

$$\dot{\vec{\gamma}} = \mathbf{A}_\gamma\vec{\gamma} + \mathbf{B}_\gamma\theta \tag{5.11}$$

This is the equation describing the dynamics of the vortex sheet.

- the expression for equation 4.3 requires the same kind of analysis as that above. Looking at the homogeneous part of the solution, different spatial wavelengths are also traveling downstream with different velocities and also growing at different velocities. This can be represented by the matrix expression:

$$\dot{\vec{w}}(x,t) = \mathbf{F}^{-1}\mathbf{H}(\alpha(\omega),U)\mathbf{F}\vec{w}(t) \tag{5.12}$$

The matrix $\mathbf{F}$ simply resolves a discrete time signal into its frequencies (i.e. compute the discrete time Fourier transform). The matrix $\mathbf{H}(\alpha(\omega), \mathbf{U})$ is a diagonal matrix with each element of the diagonal representing the equation below which must be satisfied by the corresponding spatial frequency, k,

$$\frac{d}{dt}w(k,t) = [\alpha(\omega) - i\omega]w(k,t) \tag{5.13}$$

From equation 2.29.

The driven response of this displacement can be got from equation 4.2 and is given by:

$$\frac{d}{dt}w(x,t) = -\frac{\Gamma x}{2\pi(x^2+h^2)} - \frac{1}{2\pi}\int_0^\infty \frac{\gamma(\hat{x},t)(\hat{x}-x)}{(\hat{x}-x)^2+h^2}d\hat{x} \tag{5.14}$$

Substituting for Γ and replacing the convolution integral with a matrix, we get the following expression for the homogeneous and the driven system

$$\dot{\vec{w}}(t) = \mathbf{F}^{-1}\mathbf{H}\mathbf{F}\vec{w}(t) + \mathbf{A}_{\mathbf{w}\gamma}\vec{\gamma}(t) + \mathbf{B}_{\mathbf{w}}\theta \tag{5.15}$$

This can be written as

$$\dot{\vec{w}}(t) = \mathbf{A}_{\mathbf{w}}\vec{w}(t) + \mathbf{A}_{\mathbf{w}\gamma}\vec{\gamma}(t) + \mathbf{B}_{\mathbf{w}}\theta \tag{5.16}$$

This is the equation describing the dynamics of the shear layer.

Combining the equations describing the dynamics both of the shear layer and the vortex sheet,

$$\begin{bmatrix} \dot{\vec{w}}(t) \\ \dot{\vec{\gamma}}(t) \end{bmatrix} = \begin{bmatrix} \mathbf{A}_{\mathbf{w}} & \mathbf{A}_{\mathbf{w}\gamma} \\ \mathbf{0} & \mathbf{A}_{\gamma} \end{bmatrix} \begin{bmatrix} \vec{w}(t) \\ \vec{\gamma}(t) \end{bmatrix} + \begin{bmatrix} \mathbf{B}_{\mathbf{w}} \\ \mathbf{B}_{\gamma} \end{bmatrix} \theta(t) \tag{5.17}$$

$$\vec{y}(t) = \begin{bmatrix} \mathbf{I} & \mathbf{0} \end{bmatrix} \begin{bmatrix} \vec{w}(t) \\ \vec{\gamma}(t) \end{bmatrix} \tag{5.18}$$

The second equation follows from the fact that the states of the vortex sheet will not be measured in the experiment.

This is a set standard matrix system equations. Optimum controllers for such systems have been solved for. They both stabilize the system and ensure that the some norm of the transmission from disturbances to output states is minimized. Since not all the state variables are available for feedback, the optimum controller is dynamic and involves the estimation of the states. In our case, this is inconvenient because the number of states to be estimated is large so this would take a lot of time and memory. Thus static output feedback is preferred.

5.5 Conclusion

We have come up with a method for constructing finite dimensional models for the infinite dimensional system. These are useful since only the parameters $\alpha(\omega)$ and U are identified from the system and the state space system must be reconstructed from this in order to implement multi-variate control.

We have also shown what kind of approximations are made in the process of doing this and demonstrated that they are small.

Chapter 6

Results

This is a description of the experimental procedure, the results and the comparison of the results with the prediction of the model.

6.1 Description of the Experiment

6.1.1 Input Signal

The airfoil was driven with a swept sine wave in order to identify the transfer function. The wave is of the form:

$$x(t) = sin(\frac{1}{2}at^2) \tag{6.1}$$

This is a sine wave whose frequency changes linearly with time (i.e. frequency $= \frac{d\phi}{dt} = at$). The reason this input waveform was chosen is because it has equal energy at all frequencies and it is easy to look at the output and see if it is tracking the changing excitation frequency. This is a useful feature when deciding on the magnitude of the excitation. Figure 6-1 shows the power spectral density of the input signal. Its energy remains roughly constant through all the frequencies that were excited.

Another tool that proved invaluable is the spectogram. This is a plot showing how the power spectral density of a signal changes through time. Since it has both frequency and time as its axis, it is a three dimensional plot so it will be represented as a contour plot. Figure 6-2 shows the spectogram of the input signal. As expected,

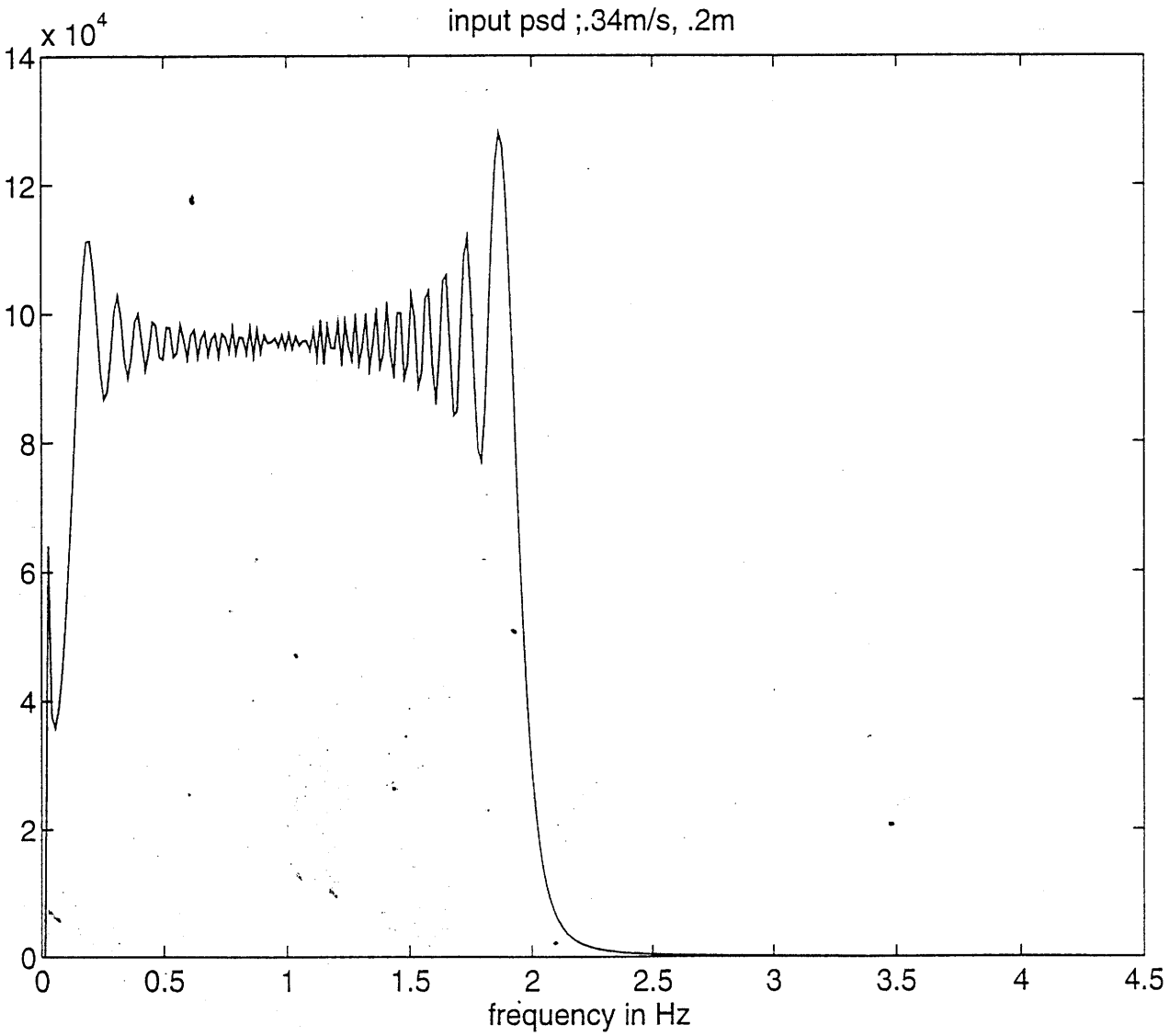

Figure 6-1: Input Power Spectral Density

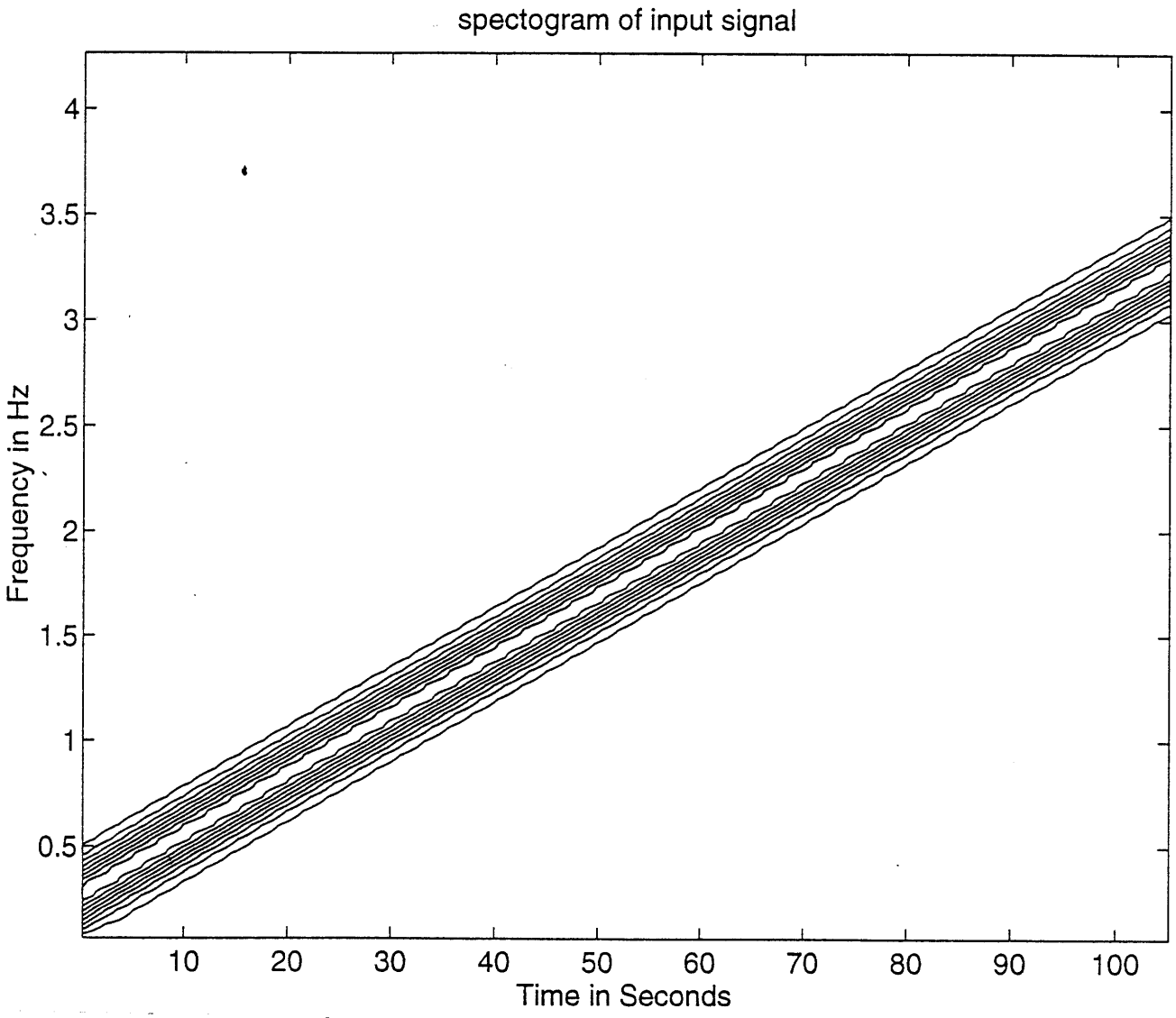

Figure 6-2: Input Signal Spectogram

at any one time the energy is concentrated in a narrow band of frequencies. The frequencies being excited also change linearly through time. By taking a spectogram of the output resulting from this input, we can tell whether the system tracked the input signal at all and also whether its response was linear.

In all runs, the camera was held about $30cm$ from the tunnel, and aimed directly at the shear layer. Because of errors both in positioning the camera and in angling it so that it was pointed directly at the fluid boundary, there were changes in the scale of the measurements of distances. These errors resulted in the errors in the velocity shown in table 6.2.

6.1.2 Data collection procedure

The system was driven with the input described above and output data was collected using the camera. Each experiment was run ten times in order to average out noise that was uncorelated with the input. Each run took 120 seconds to complete (20 minutes for an experiment) and resulted in 1024 time samples of data being collected for a total of 25 points on the screen. Because of difficulty collecting and storing all this data, the ten runs were averaged while the experiment was being conducted and this average was stored. The coherence between the 10 different runs of the experiment could not be computed as only the average of the data was stored.

In all runs, the camera was held about $30cm$ from the tunnel, and aimed directly at the shear layer. Because of errors both in positioning and aiming the camera at the fluid boundary, there were changes in the scale of the measurements of distances. Because of these errors, estimates of the velocity of the shear layer in two experiments with the tunnel at the same speed do not agree because the scale of the measurements is changed as a result of the positioning of the camera. This explains table 6.2. The computer collected data at 25 points on the screen. These points were separated from each other by .6 inches.

Because the camera had a limited range, each experiment was done twice:

- with the camera $20cm$ from the airfoil (near)

- with the camera $90cm$ from the airfoil (far)

This made the detection of subtle changes in the wave as it convected possible. This is especially important because we are looking for waves which grow exponentially as they convect.

The system is expected to get more unstable as the flow velocity is increased. In order to detect how changes in velocity affect the shear layer, the experiment was done with the tunnel running at three different speeds:

- fast: .485 m/s
- medium: .46 m/s
- slow: .34 m/s

The speeds listed above are the estimated velocities of the shear layer disturbances. Theory (see chapter 2) suggests that these velocities are half of the velocity of the tunnel but the tunnel was not instrumented to measure the velocity so the actual velocity was not measured. These velocities are simply the means of the velocities in table 6.2. An explanation of how they were computed comes later.

6.2 Effect of the Airfoil on the Shear layer

If the airfoil is to be used to control the shear layer, it is important that it enjoy a significant amount of control authority. A measure of the control authority is the coherence of the shear layer at points close to the airfoil to the motion of the airfoil. This shows how much of the motion of the shear layer is due to the airfoil. As previously explained, the coherence cannot be computed because all the averaging was done while the data was being collected. Since the input only has one frequency at any time and this frequency changes linearly with time, we can get an idea of how good the coherence is by checking to see that the shear layer tracks the frequency of the airfoil.

One way to do this is to look at the time history of the shear layer and to see if it tracks the frequency of the input. It is easier to do using the spectogram. Because

the peak of the spectogram of the input follows a straight line (this follows because the frequency of the input increases linearly with time), the linear response from this input should have the frequency increase monotonically with time. Since the actuator dynamics are much faster than the driving frequencies, the delays to the different frequencies should be almost the same. This means that the response to the input should have the frequency increasing linearly with time. This looks like a diagonal ridge on a plot of frequency against time.

The spectogram, being a contour plot of a three dimensional figure does not give insight into the nature of the transfer function or its magnitude. Difficulty in labelling the third dimension makes this almost impossible. However, the ease with which one can extract features such as the diagonal ridge that we are looking for make it useful in visualizing the coherence as a function of frequency.

In order to qualitatively estimate the coherence between the point closest to the airfoil at which data was taken and the airfoil, the spectogram of this point was compared with that of the input. By looking to see if this point tracked the input, an estimate of the quality of the actuation was made.

6.2.1 Effect of Airfoil with tunnel at high speed

Figure 6-3 shows the spectogram of the displacement of the shear layer close to the airfoil with the tunnel running at approximately .485m/s. The diagonal response at the lower frequencies shows that the shear layer tracked the airfoil at these lower frequencies. This is equivalent to saying that there is good coherence between the input and the output at these low frequencies. However, this coherence stops at about 1.6 Hertz. Above this frequency, the linear response to the input frequency becomes less important than the non-linear response. This is why most of the energy is off the diagonal.

Because of this non-linear response of the shear layer to the airfoil, the airfoil can only be used to control the airfoil so long as the frequencies of the airfoil are low enough that they do not cause a non-linear reaction. The non-linear reaction is especially bad because it affects the low frequencies that cohere well with the input

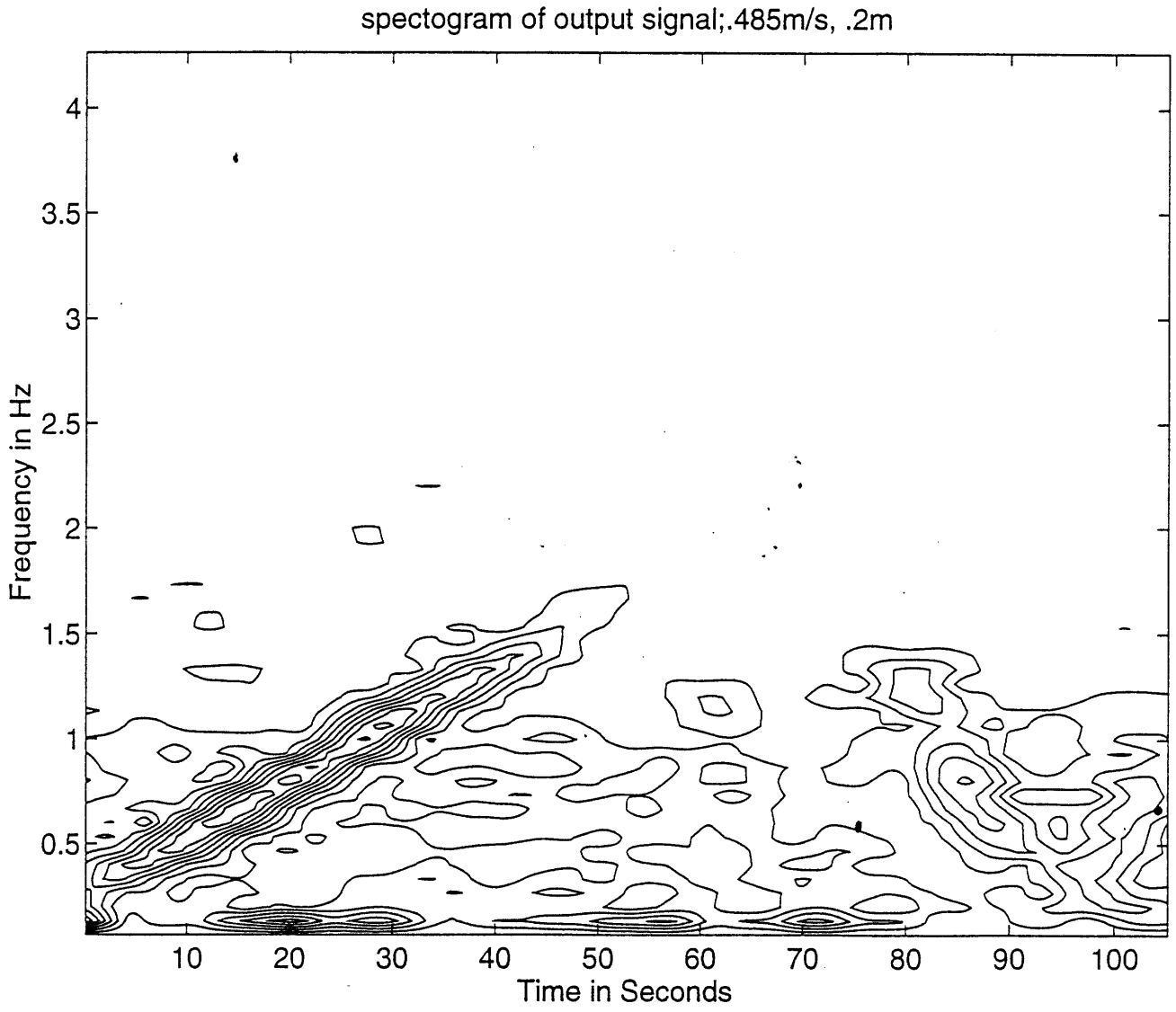

Figure 6-3: Output Spectogram at approximately .485m/s close to airfoil

data.

Figure 6-4 shows the equivalent spectogram to figure 6-3 except that now it is taken far from the airfoil. The only difference is that now the energy seems to become concentrated at one frequency. There is no increase in the off-diagonal non-linear effects which means that maybe the shear layer evolves in a linear fashion.

6.2.2 Effect of Airfoil with tunnel at medium speed

Figure 6-5 shows the spectogram of the displacement of the shear layer close to the airfoil with the tunnel running at medium speed. As is the case with the tunnel at approximately .485m/s, the diagonal response at the lower frequencies shows that the shear layer tracked the airfoil at these lower frequencies showing good coherence at these low frequencies. However, this coherence stops at about 1 Hertz. Above this frequency, the linear response to the input frequency becomes less important than the non-linear response. This is why most of the energy is off the diagonal. As the tunnel is slowed down, there is a loss in the controllability of higher frequencies. This means that the airfoils are an even worse method of control for the system at this lower velocity.

Figure 6-6 shows the equivalent spectogram to figure 6-5 except that now it is taken far from the airfoil. It appears that the energy at a certain band of frequencies has become relatively higher. There is no evidence of an increase in non-linearity.

6.2.3 Effect of Airfoil with tunnel at slow speed

Figure 6-7 shows the spectogram of the displacement of the shear layer close to the airfoil with the tunnel running at a slow speed. The output coheres with the input only at very low frequencies. This coherence stops at 0.8 Hertz. Above this frequency, the linear response to the input frequency becomes less important than the non-linear response. This is why most of the energy is off the diagonal. At this low speed, the airfoil would be an ineffective method of controlling the airfoil.

Figure 6-8 shows the equivalent spectogram to figure 6-7 except that now it is

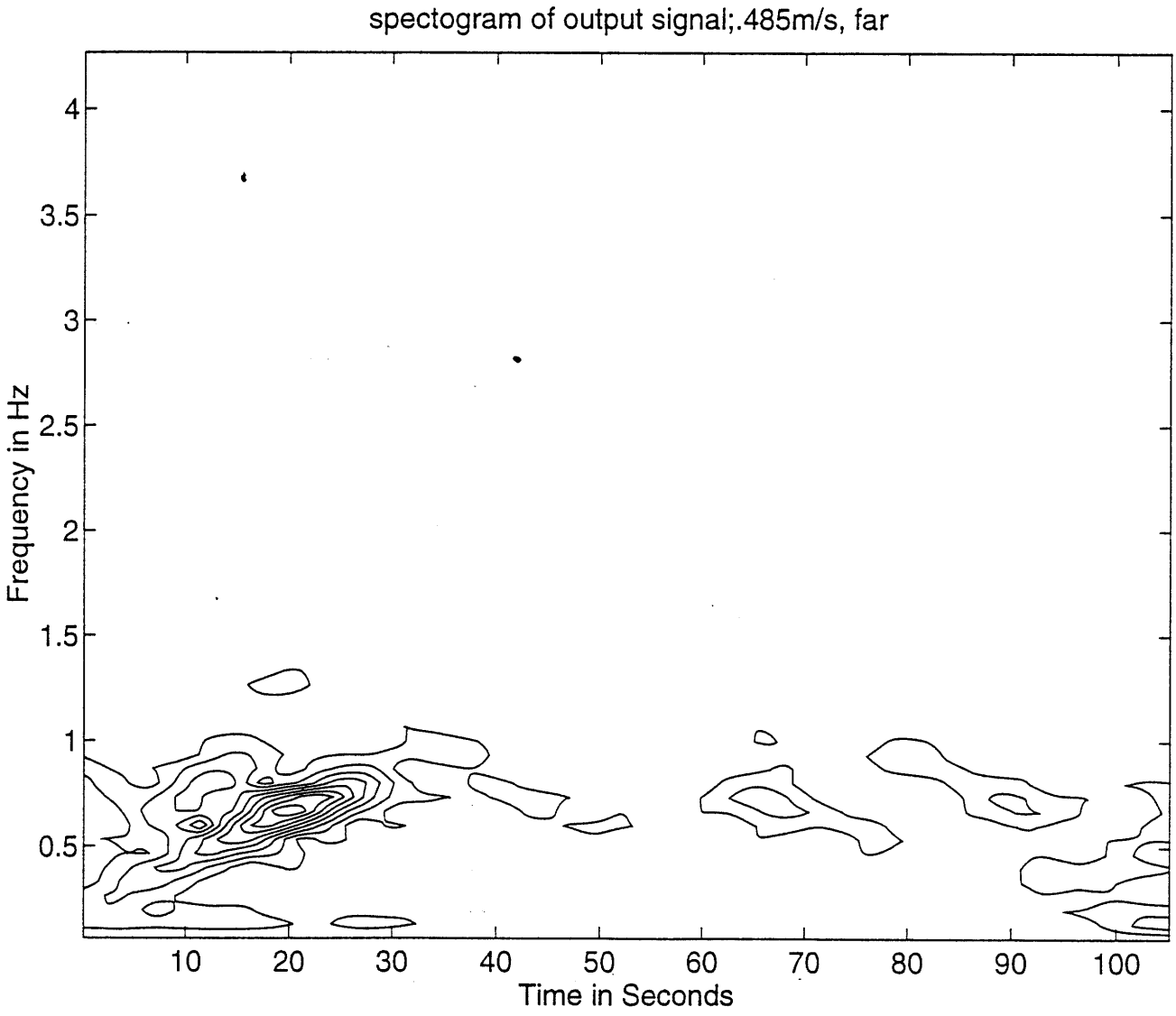

Figure 6-4: Output Spectogram at approximately .485m/s far away from airfoil

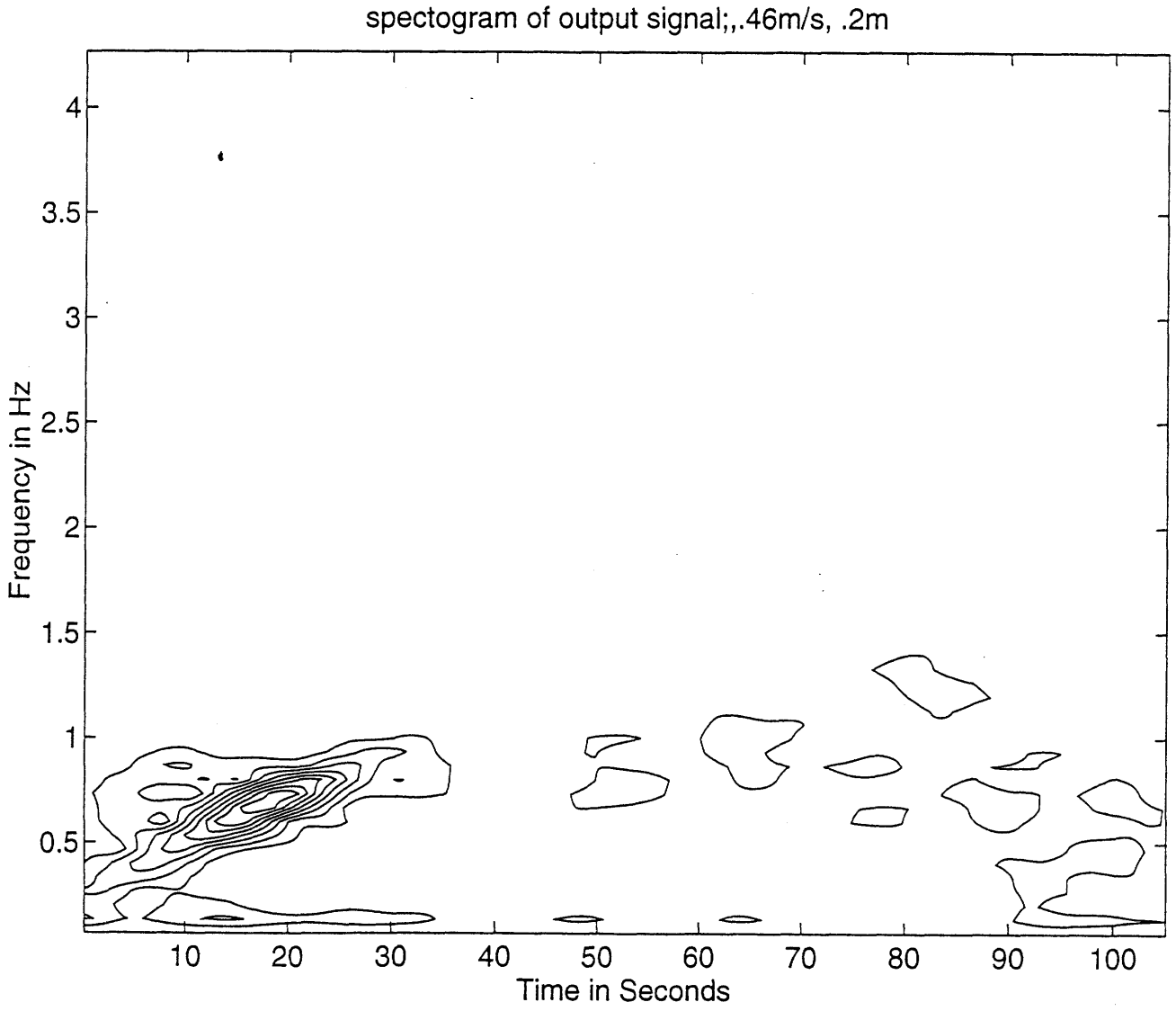

Figure 6-5: Output Spectogram at approximately .46 m/s close to airfoil

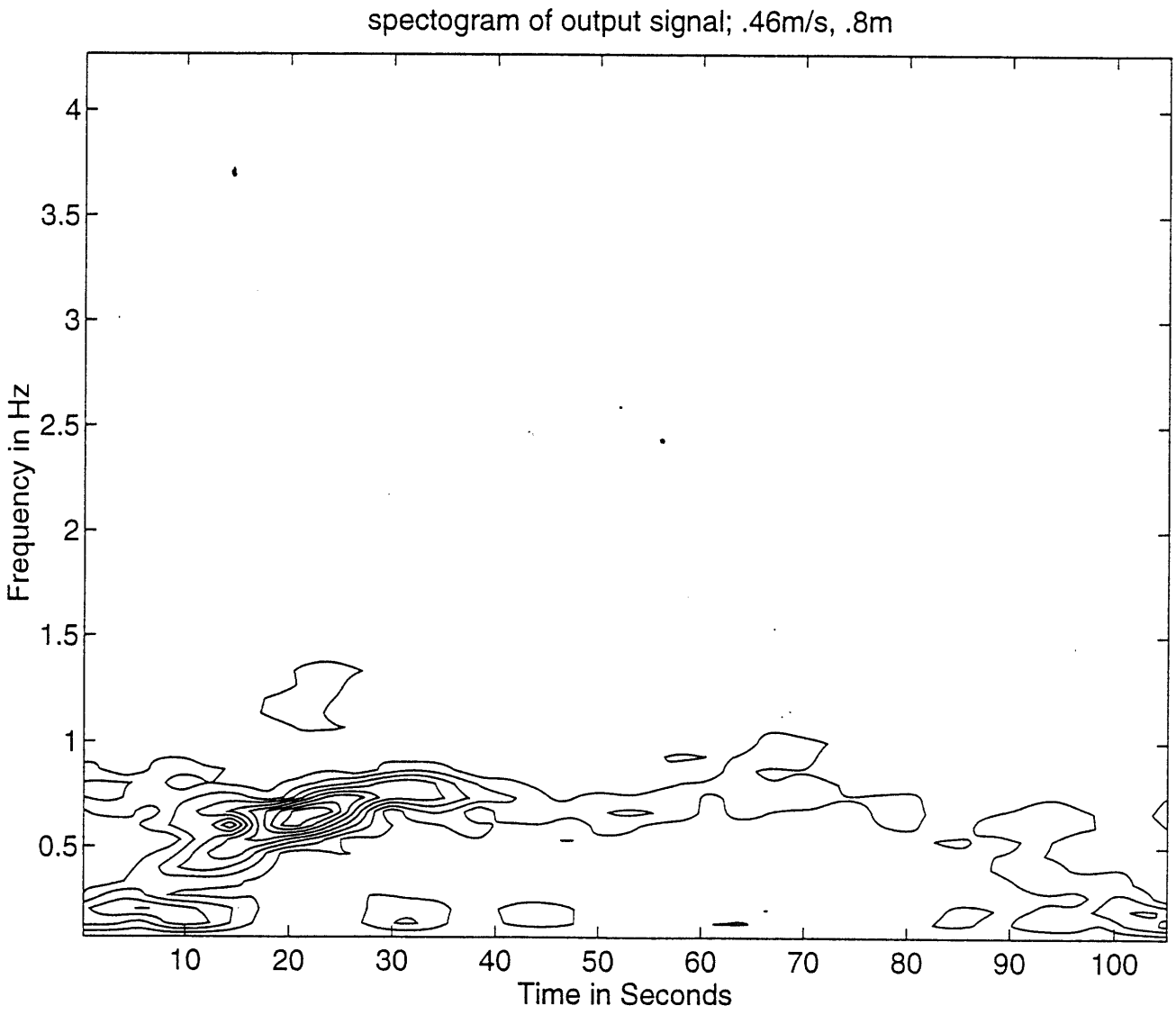

Figure 6-6: Output Spectogram at approximately .46 m/s far away from airfoil

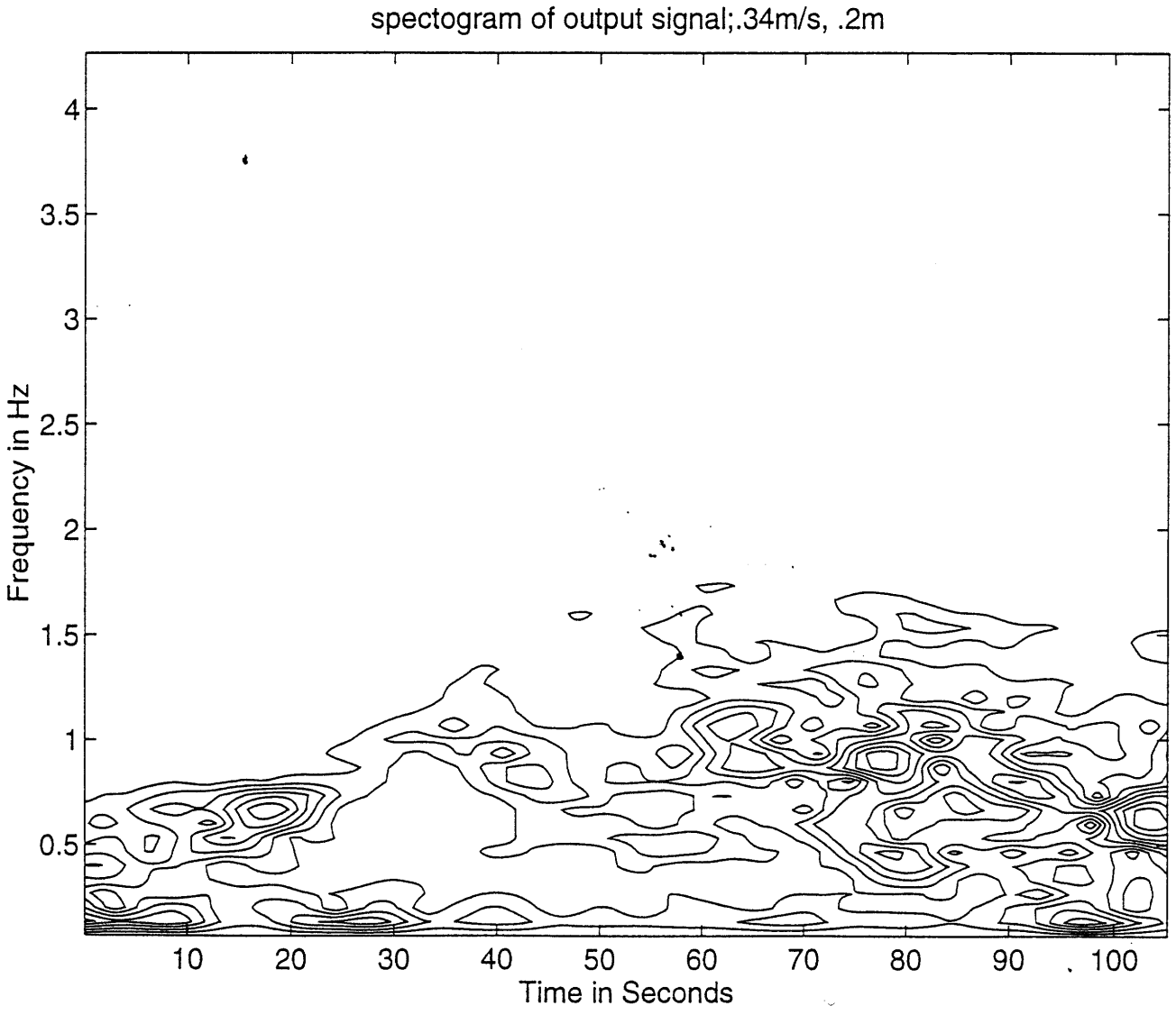

Figure 6-7: Output Spectogram at slow speed close to airfoil

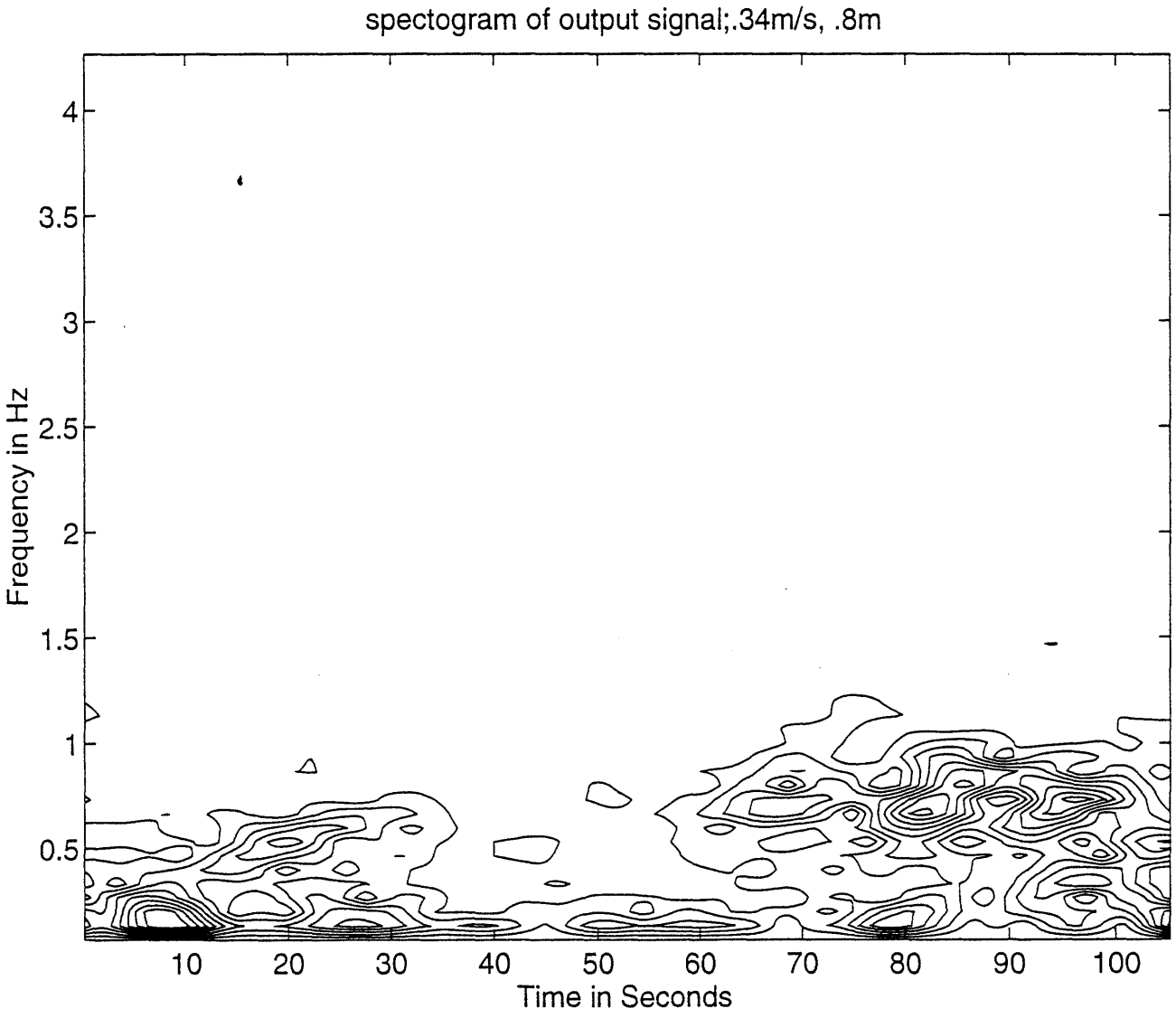

Figure 6-8: Output Spectogram at approximately .34 m/s far away from airfoil

velocity(ms^{-1})	frequency (Hz)	$Re_\lambda = \frac{U^2}{\omega\nu}$
.48	1.6	$8X10^4$
.456	1	$12X10^4$
.343	.8	$8.17X10^4$

Table 6.1: Table of highest frequency of linear response at different velocities

taken far from the airfoil. The band of frequencies that responded linearly can still be seen. However, just like in the previous plot, most of the energy goes towards evoking a non-linear response.

6.2.4 Conclusion

The airfoil is only effective in evoking a linear response in the shear layer at frequencies below a certain threshold. Above this threshold, the energy excites a lower frequency than the input through some non-linear mechanism.

The table above gives the highest frequency excited for the different tunnel velocities. As shown in table 6.1, the highest frequency at which a linear response is discernible reduces as the tunnel is slowed down. Because the frequencies convect at a constant rate, this highest temporal frequency corresponds to a spatial frequency given by $\frac{U}{\omega}$. The third column gives the Reynolds number with respect to this frequency. As is evident in the table, for each velocity, the last frequency that is linear occurs at approximately the same Reynolds number with respect to its spatial frequency. This seems to imply that the non-linearity is a result of viscosity which we assumed to be zero in the analysis.

6.3 Homogeneous dynamics

The purpose behind the experiment is to study the shear layer and not the airfoil. This is what the rest of this section concentrates on.

The data collected contained the output history for 25 points. These points were divided into four sets. Since the transfer function from one point to others on the shear layer should be invariant to shifts along the length of the shear layer, it should

be the same for all four data sets. By averaging these four data sets, an estimate of the transfer function was calculated. A measure of the coherence of this transfer function was also calculated.

6.3.1 Convection Velocity

One of the two major predictions of the linear model is that all frequencies in the shear layer will convect with the same group velocity. This means that disturbance will travel downstream with the same velocity. The model also predicts that this velocity will be $\frac{1}{2}$ of the velocity of the water in the tunnel. This was checked for the tunnel. If this is the case then the output at a point downstream of another should simply be delayed. All other changes should occur in its magnitude at other frequencies.

As previously explained, each experiment collected data at 25 points. This data was divided into four groups. One group started with the 1first point, the second with the second point and so on. If one point was already in the group, the point after it was skipped and the one after that was allowed into the group etc. This resulted in the groups having 12 points. All the groups should have the same transfer function from one point to the others in the group since they are separated by the same distance. These transfer functions were computed and the coherence over the four groups calculated to see how consistent the measure of the transfer function was.

Because the experiment at approximately .485m/s resulted in the excitation of the most frequencies, the data at approximately .485m/s and far away from the tunnel will be used to illustrate the results.

Tunnel at approximately .485m/s far away from airfoil

As described above, the transfer function from the first point to the remaining downstream points was calculated. To demonstrate the validity of the transfer function, it is important to look at its coherence.

Figure 6-9 shows the coherence of the transfer function. downstream. The figure to the lower left shows the coherence against the position for the many different

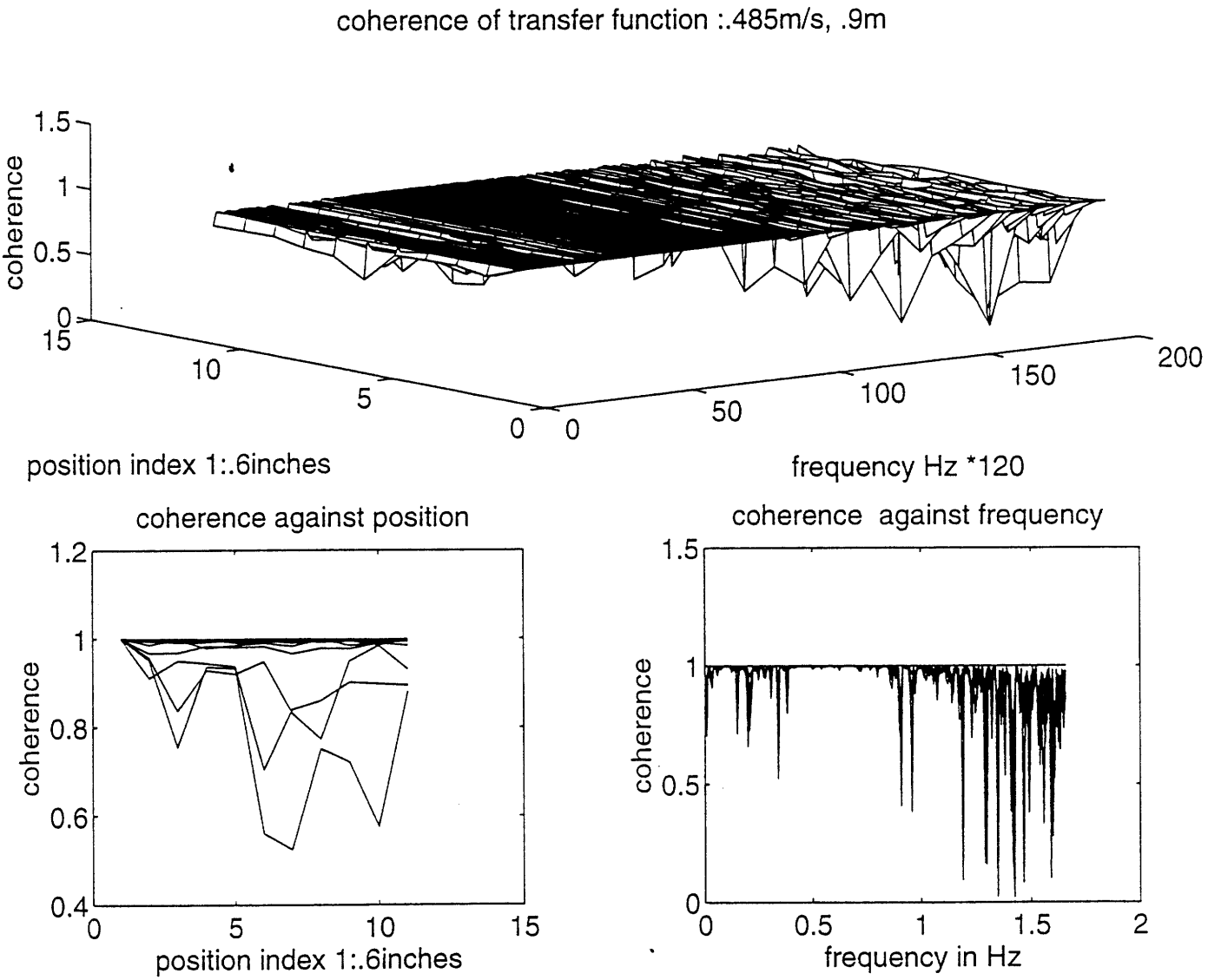

Figure 6-9: Transfer coherence as waves convect downstream: .485 m/s and .9m

frequencies. The figure to the right shows the coherence against frequency for the different points. It is clear from the figure to the right that the lower frequencies cohere very well. This indicates that we have a pretty good measure of the transfer function.

Figure 6-10 shows the changes in the angle of the transfer function at different frequencies as the wave travels downstream. The figure to the lower left shows the angle against the position for the many different frequencies. The plot shows that the angle appears to be linear. The figure to the right shows the angle against frequency for the different points. This also appears to be linear. This linear phase with position and frequency is what we expect for a convective system.(i.e. from equation 2.2, $\angle G = \angle(e^{\frac{-j\omega x}{U}})$ since the delay increases linearly with distance downstream x).

A line was fitted to each of the plots of figure 6-10. The upper plot in figure 6-11 is a plot of the slopes of these lines against frequency . The lower plot shows the mean squared error in fitting each of the slopes in the upper plot. As can be seen in the upper plot, a line fits these slopes very well. This means that the frequencies convect at the same velocity. This velocity is given by the reciprocal of the slopes of this line.

Other runs

This same analysis was done for other plots and the plots corresponding to figure 6-11 are at the end of this chapter. The velocities derived from these plots are in table 6.2. Because of sensitivity of the separation of the points at which the data is being taken to the camera position, the velocity estimates are noisy but the trends are still evident.

Note that runs at the same speed are at the same tunnel velocity but the calculated velocity varies because when the camera was moved, it was not place at the exact same position and angle. An estimate of the convection velocity can be found by averaging the two calculated velocities.

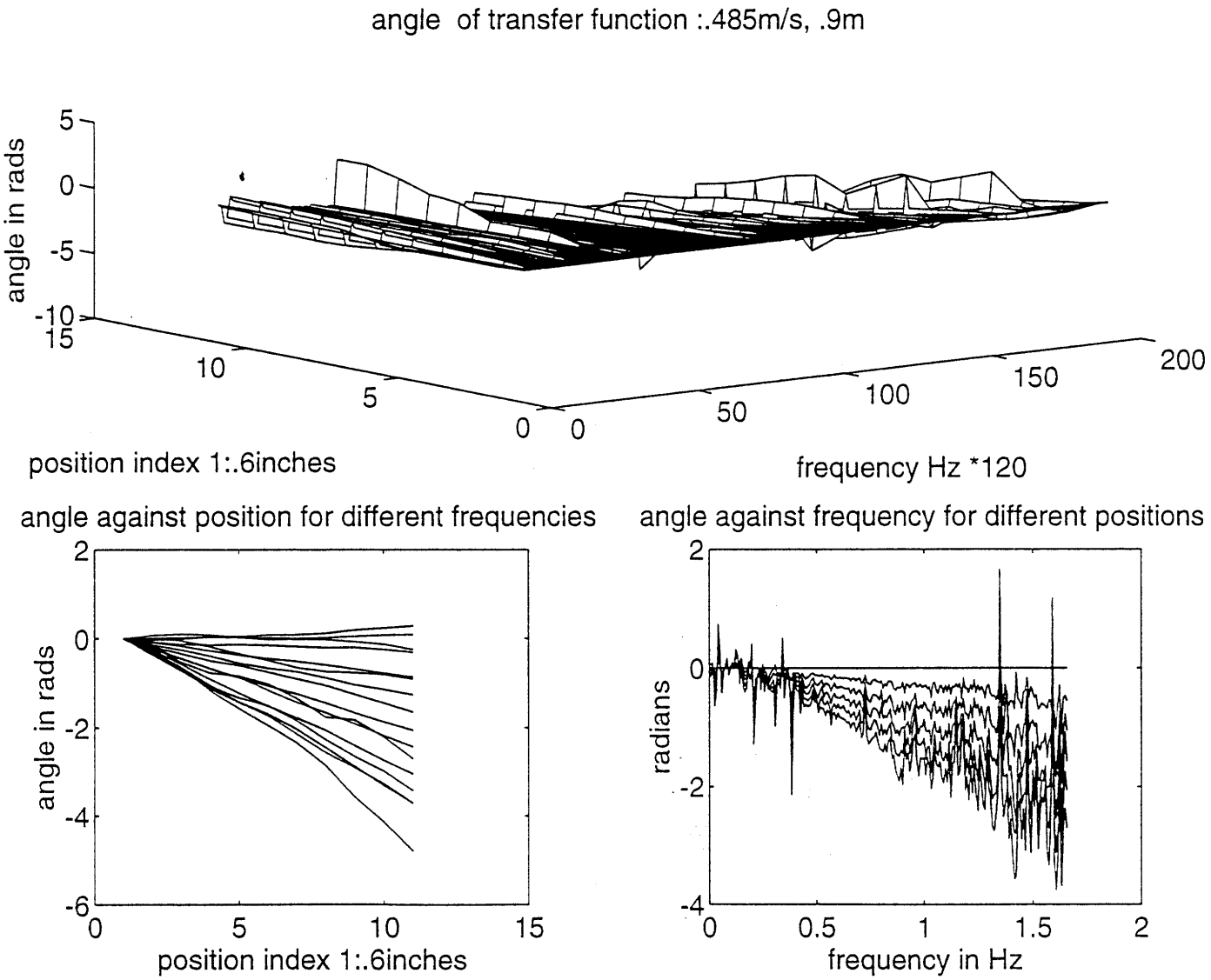

Figure 6-10: Transfer function angle as waves convect downstream: .485 m/s and .9m

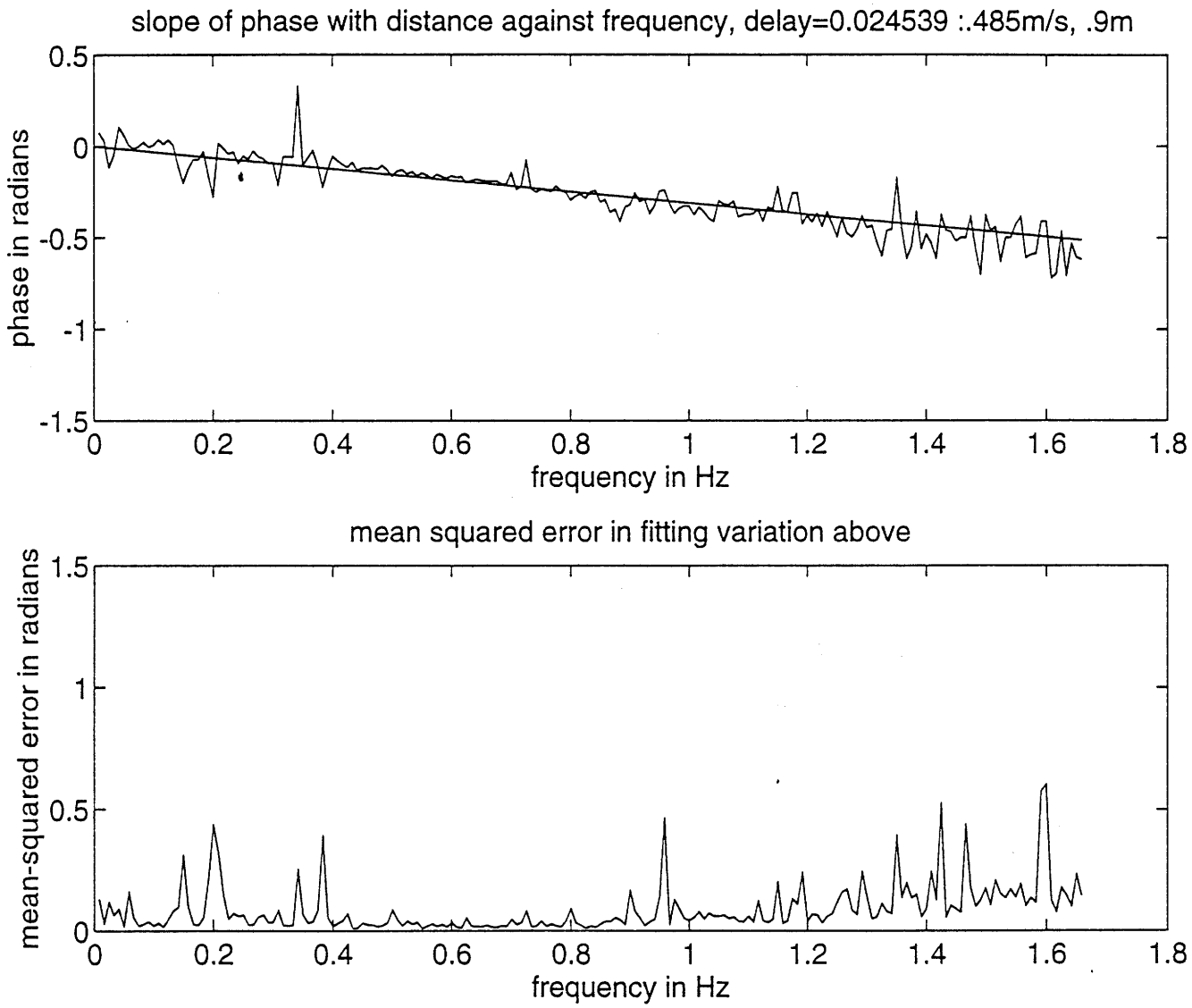

Figure 6-11: Transfer function angle slope against frequency: .485 m/s and .9m

speed	position	velocity(ms^{-1})
high	near	.4819
high	far	.4898
medium	near	.484
medium	far	.4364
slow	near	.3960
slow	far	.2896

Table 6.2: Table of convection velocity for the different runs

6.4 Changes in Amplitude

Tunnel at approximately .485m/s far away from airfoil

Figure 6-12 shows the changes in the magnitude of the wave at different frequencies as the wave travels downstream. The figure to the lower left shows absolute value of transfer function against position downstream. There is not much increase in the amplitude of the waves over the region studied. The plots against frequency show that even though certain frequencies appear to grow, the plot is very choppy and no general trends can be observed. Because of this, a comparison of data taken nearby and that taken far away had to be made to study the changes in amplitude as the waves convect.

Because 25 data points wear taken in both nearby and far away runs, there were 25 estimates of the transfer functions from a point in the first window to the corresponding point in the next window. By averaging these transfer functions, low-noise estimates of the transfer function were made and the coherence calculated. Since the nearby and far away runs were separated by 0.7 meters, the value of alpha was calculated with the assumption that the growth was exponential between the two points.

Figure 6-13 shows the transfer function and its coherence from one point to another far away. The coherence is pretty good. Based on 6.2, the logarithm of the amplitude of this transfer function gives alpha which is shown in figure 6-14. From the plot, frequencies between 0.4 and 0.8 Hertz are unstable. The instability at .1 Hz appears to be unrelated to the dynamics modeled in chapter 2 because they predict

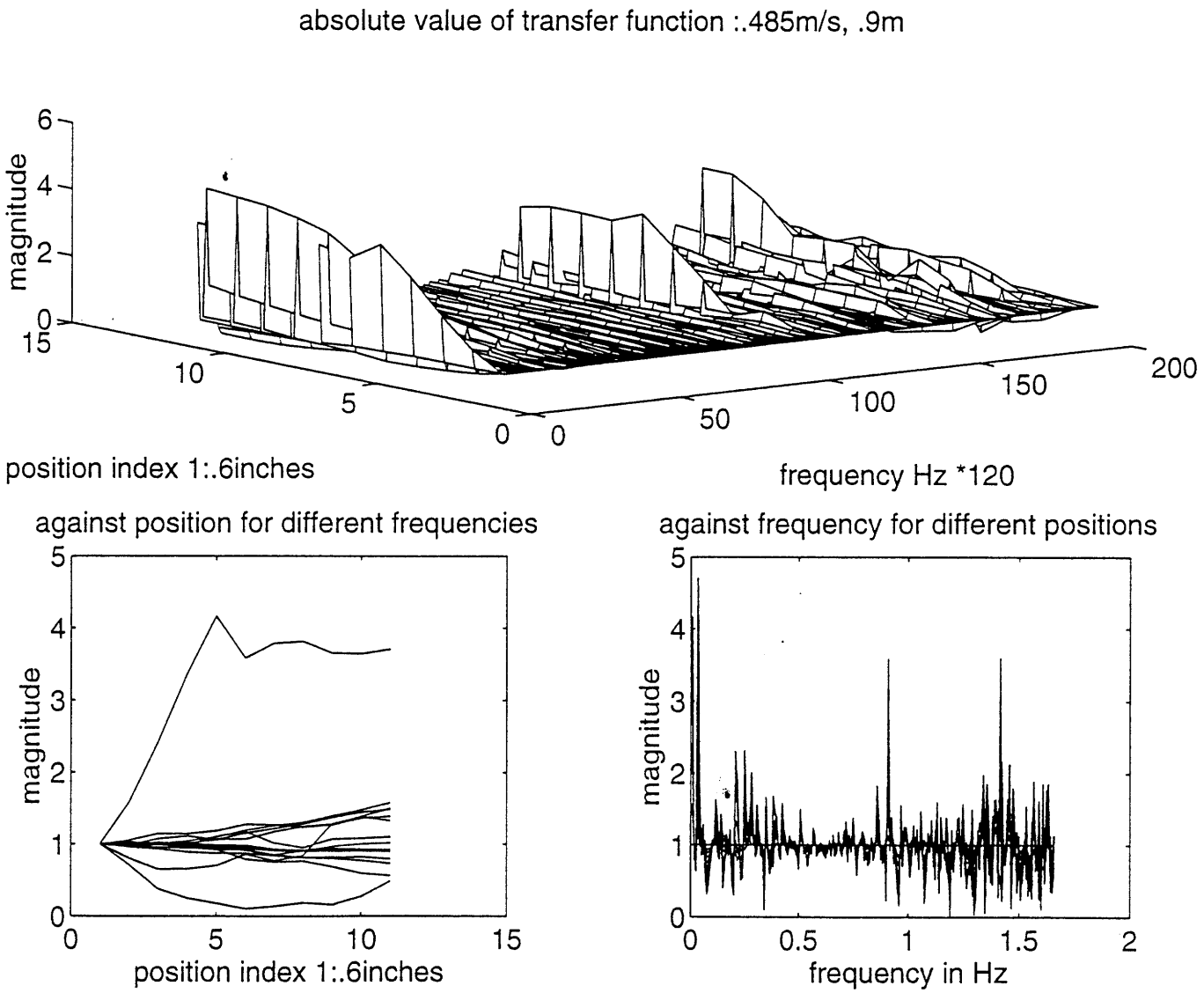

Figure 6-12: Transfer function magnitude as waves convect downstream: .485 m/s and .9m

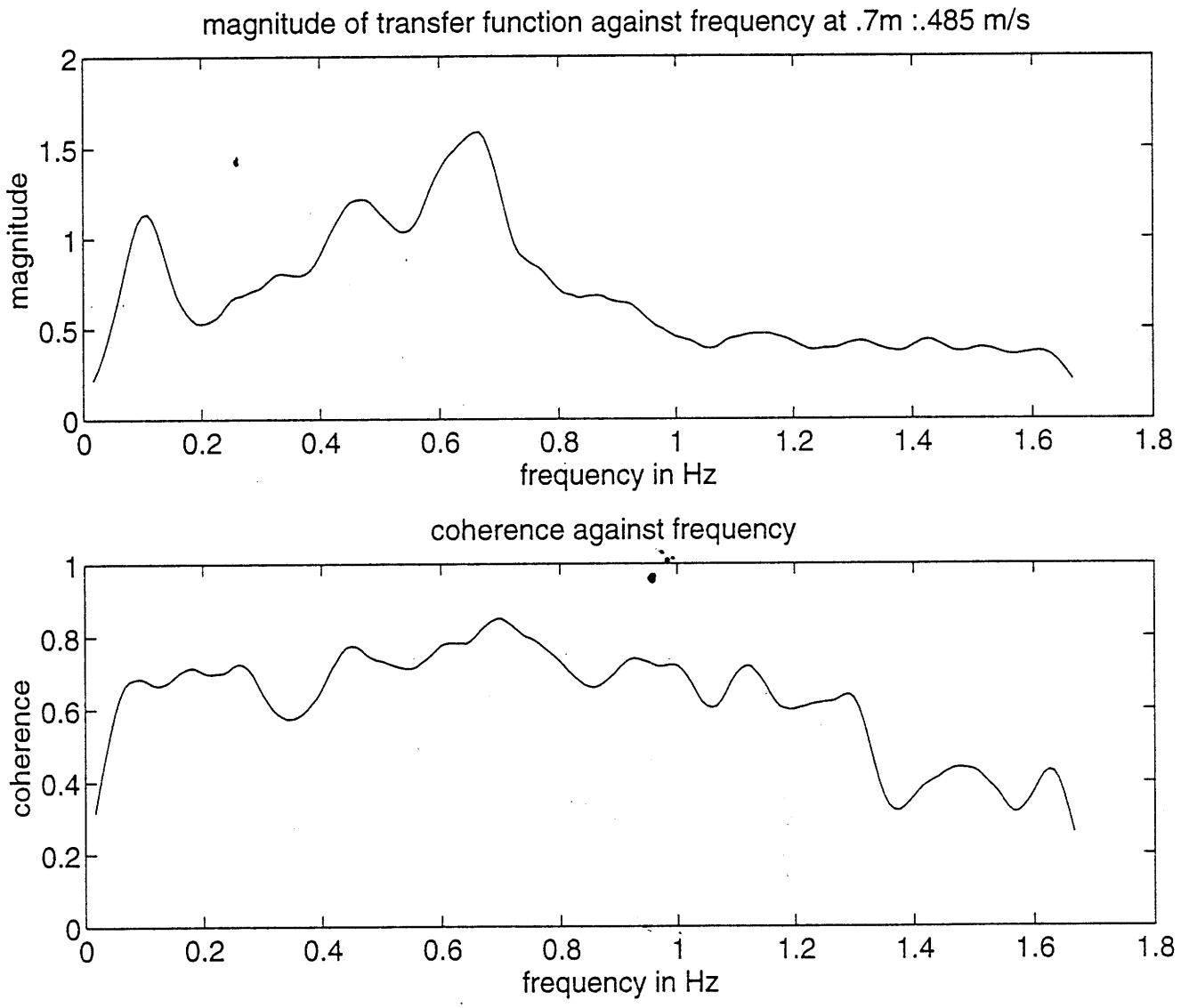

Figure 6-13: Transfer function magnitude to a point .7m away: .485 m/s

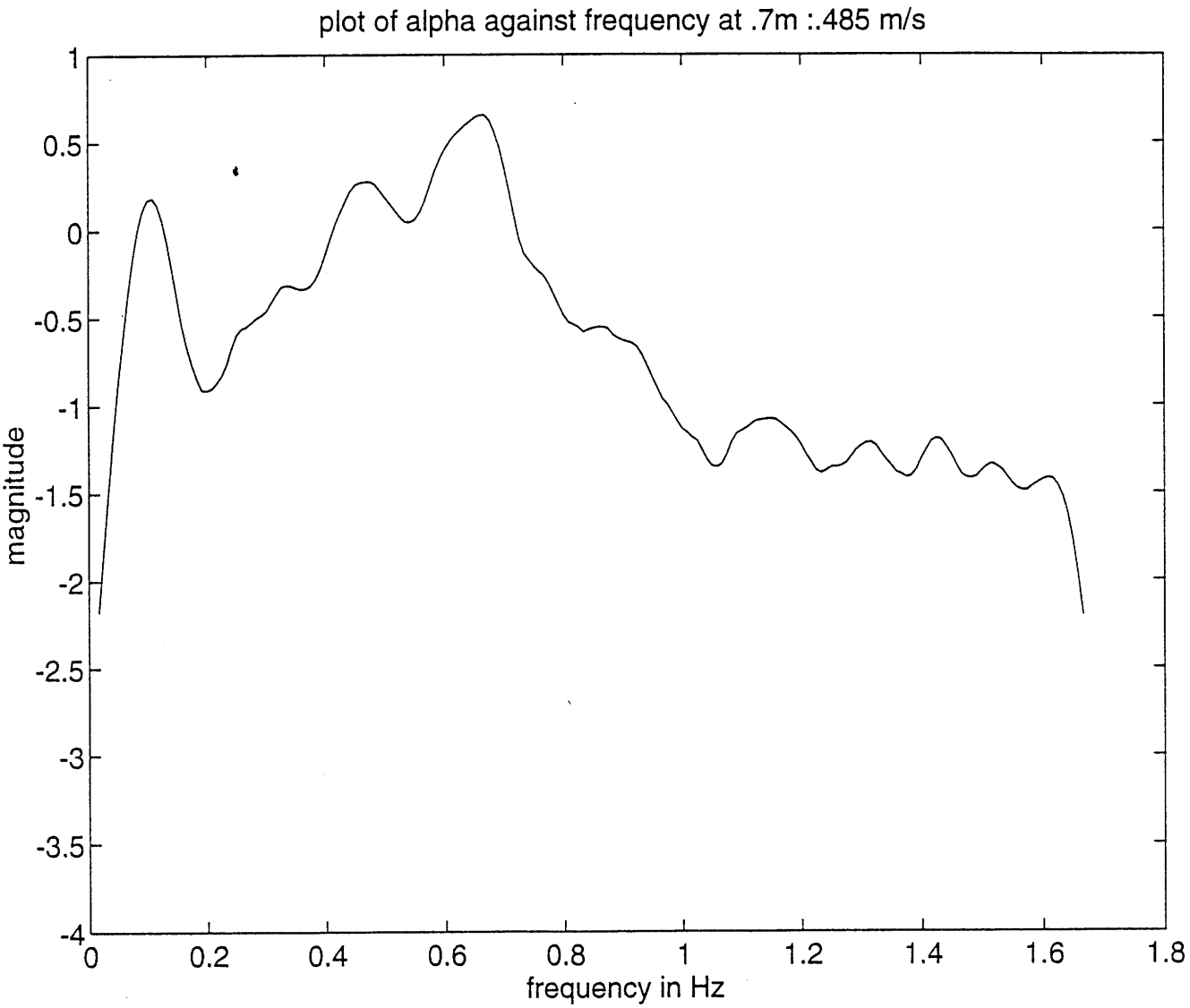

Figure 6-14: Alpha with tunnel running at .485m/s

only one instability at a higher frequency.

Figures 6-15 and 6-16 show the transfer function and coherence and also alpha with tunnel moving at a moderate velocity. At this velocity, the frequencies between .4 and .8 Hz are stable. The instability at .1 Hz still exists.

The linear model predicts that all other frequencies should be marginally stable. However, because of viscosity there is dissipation and they are strictly stable.

Figures 6-17 and 6-18 show the transfer function and coherence and also alpha with tunnel moving at a low velocity. From figure 6-17, this data has low coherence (less than .5) and very little information (if any) can be got from it.

6.4.1 Conclusion

It was demonstrated that all frequencies convect at the same velocity and that this velocity increases with tunnel velocity. It was also shown that frequencies between .4 and .8 hz become more unstable as the tunnel is sped up. Other frequencies are strictly stable instead of being marginally stable as predicted by the linear model.

With the exception of the absolute stability of stable modes, the data collected fits the expectations for the Kelvin-Helmholtz instability pretty well.

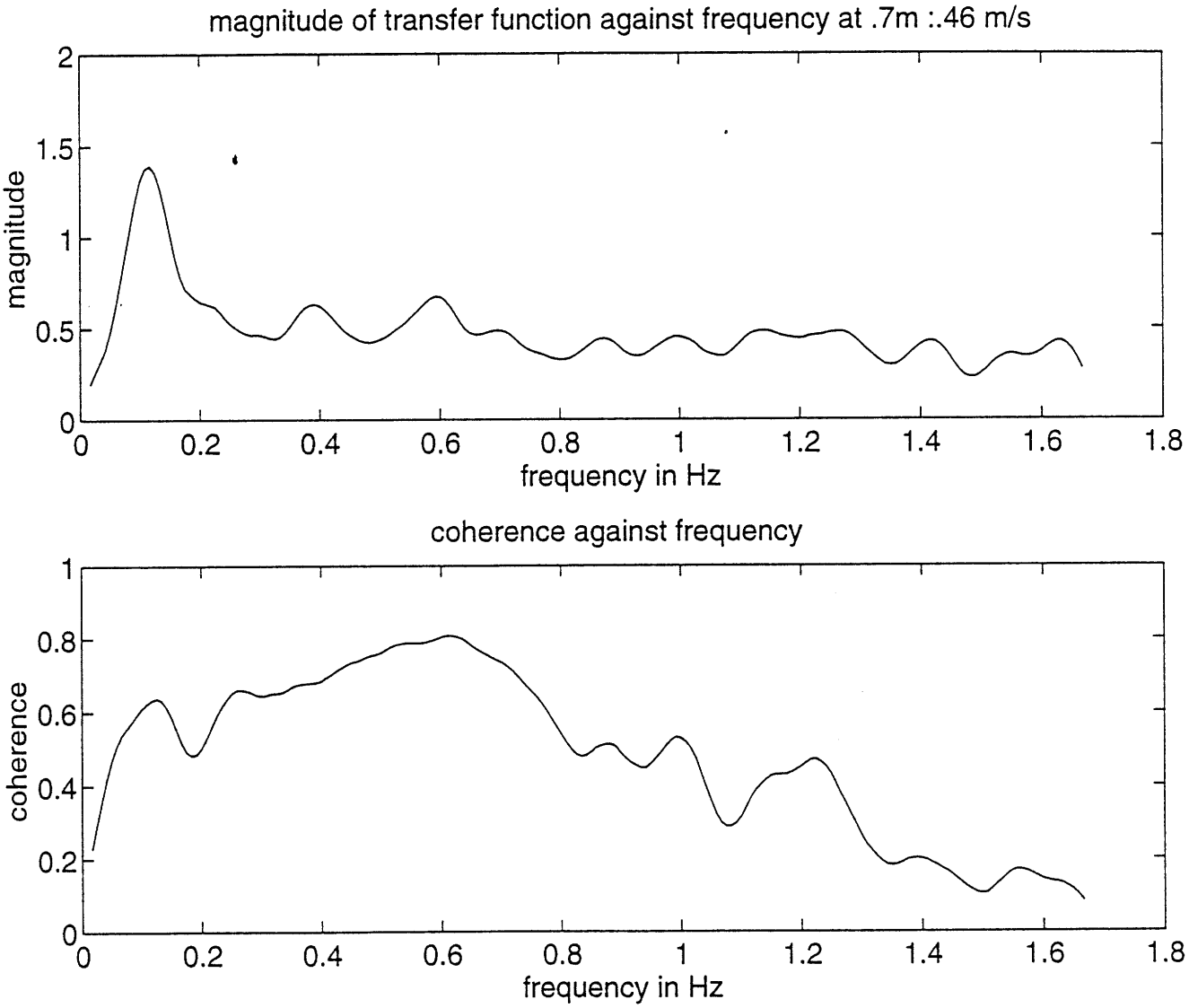

Figure 6-15: Transfer function magnitude to a point .7 meters away: .46m/s

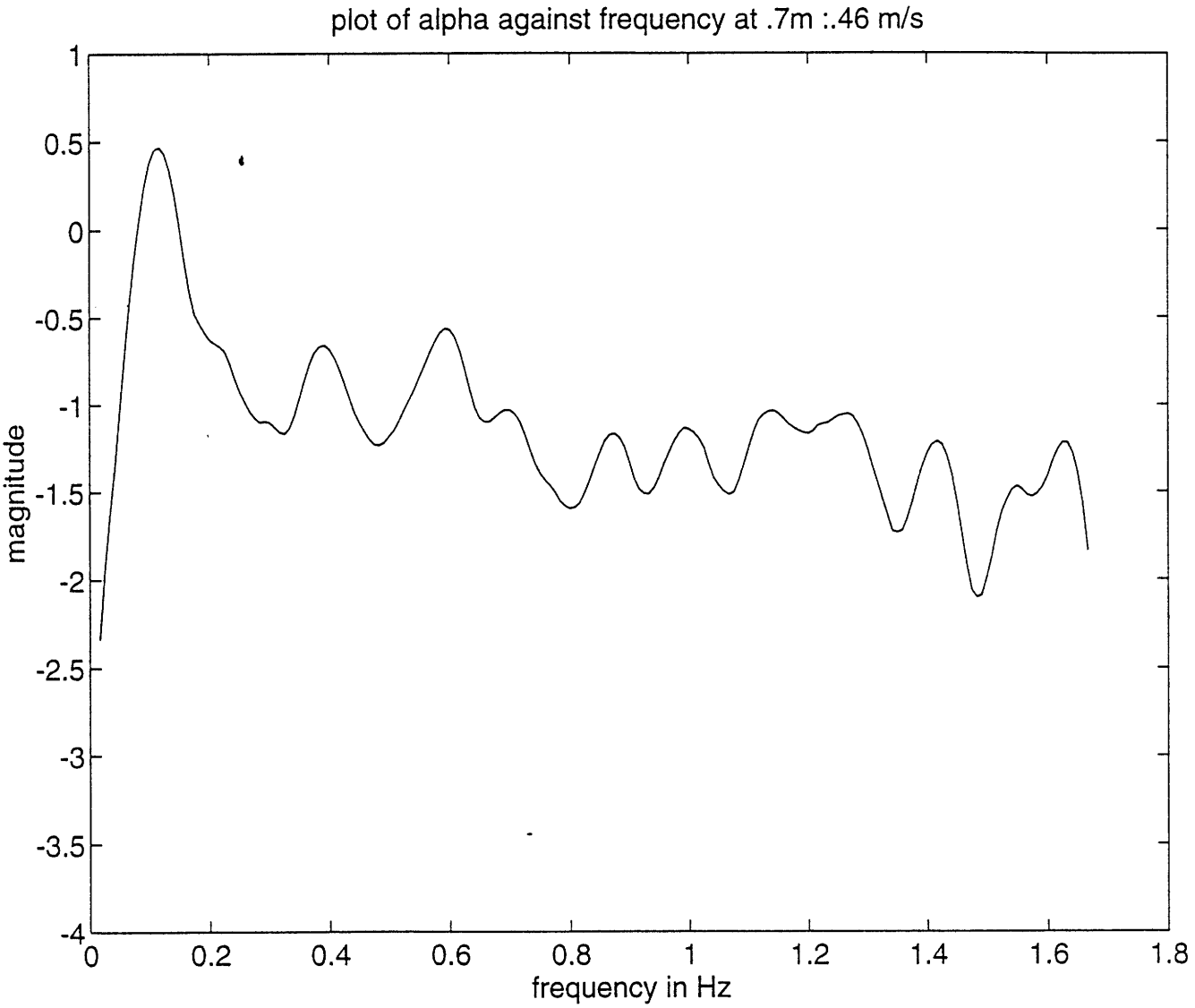

Figure 6-16: Alpha with tunnel running at .46m/s

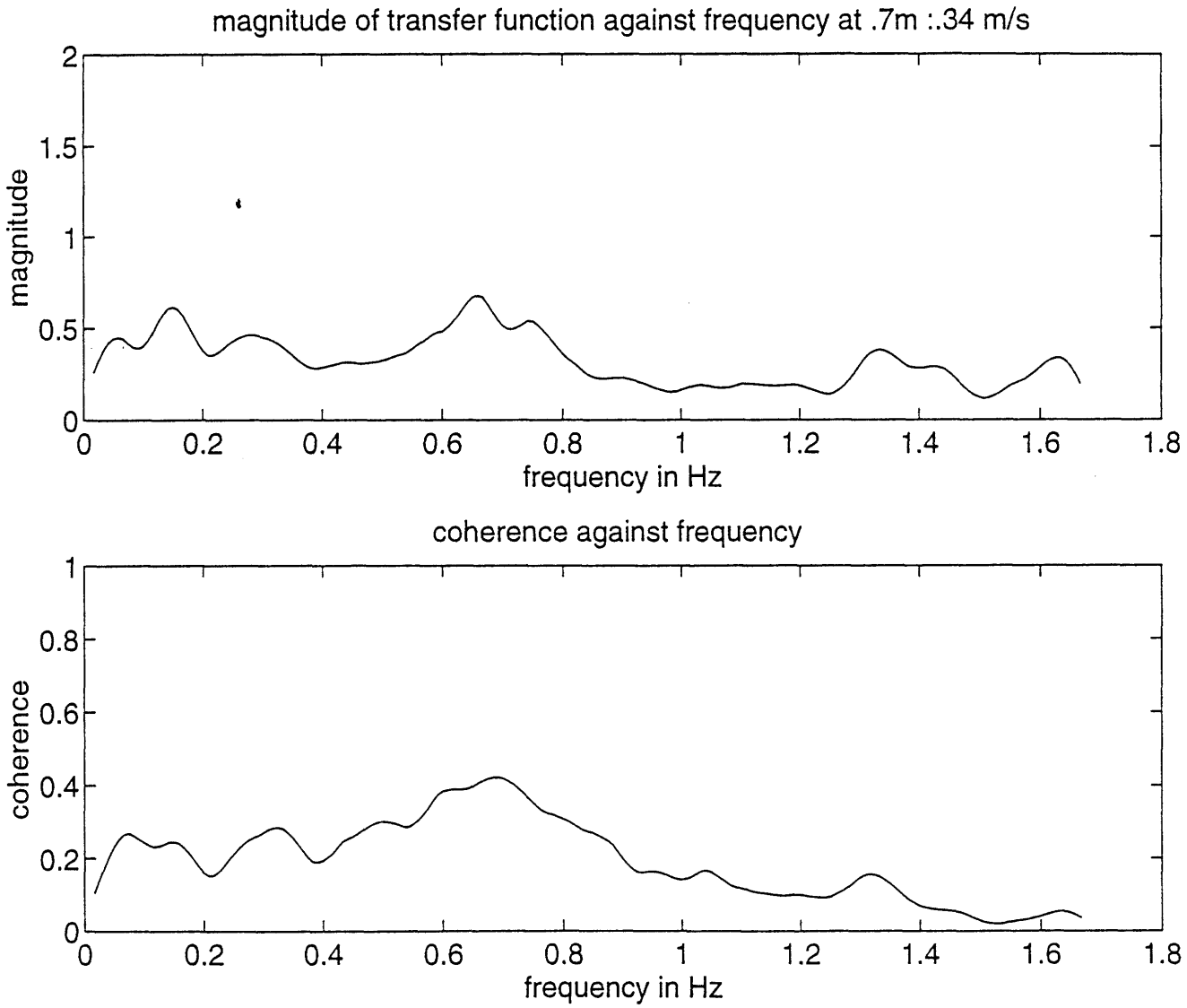

Figure 6-17: Transfer function magnitude to a point .7 meters away: .34m/s

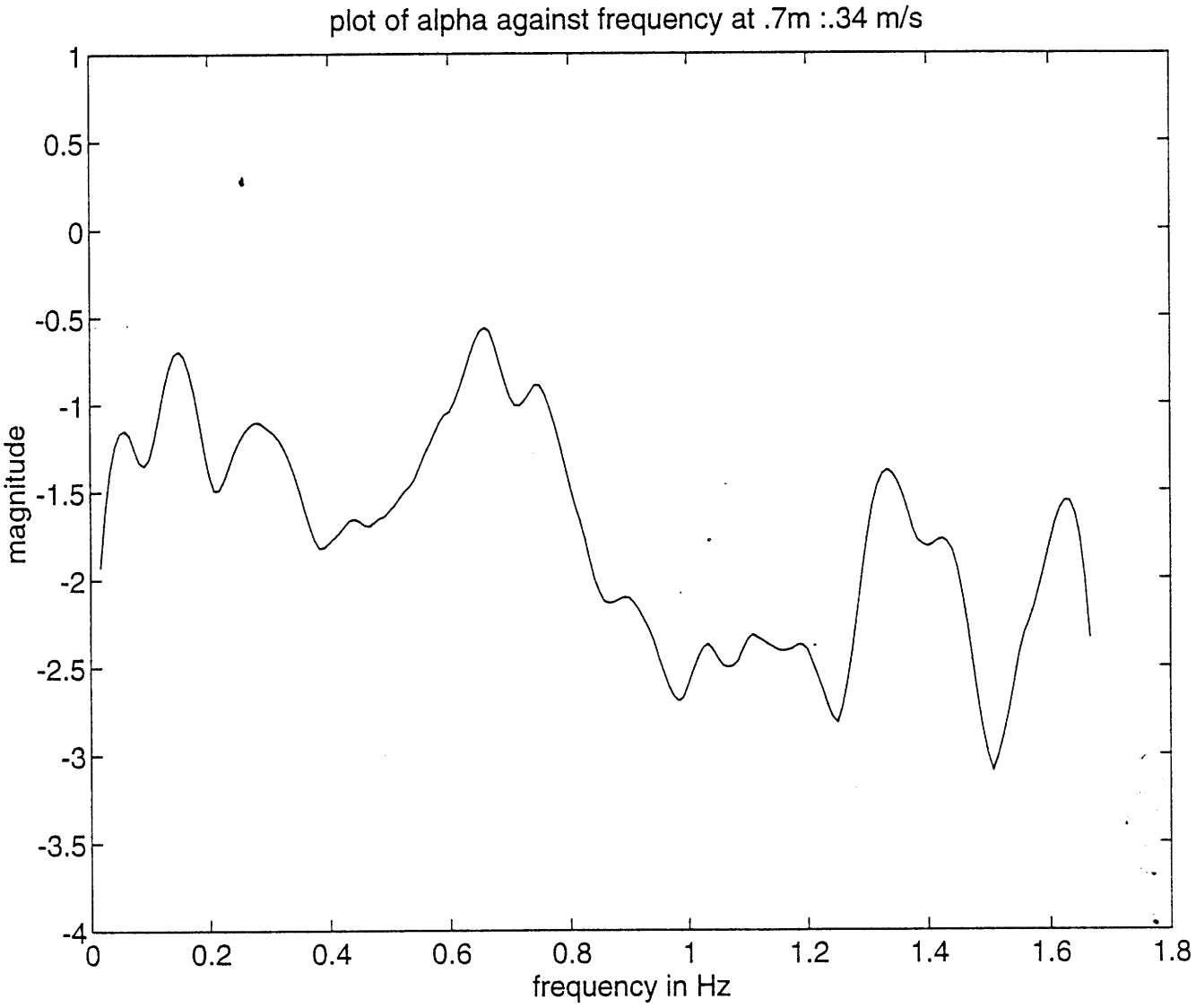

Figure 6-18: Alpha with tunnel running at .34m/s

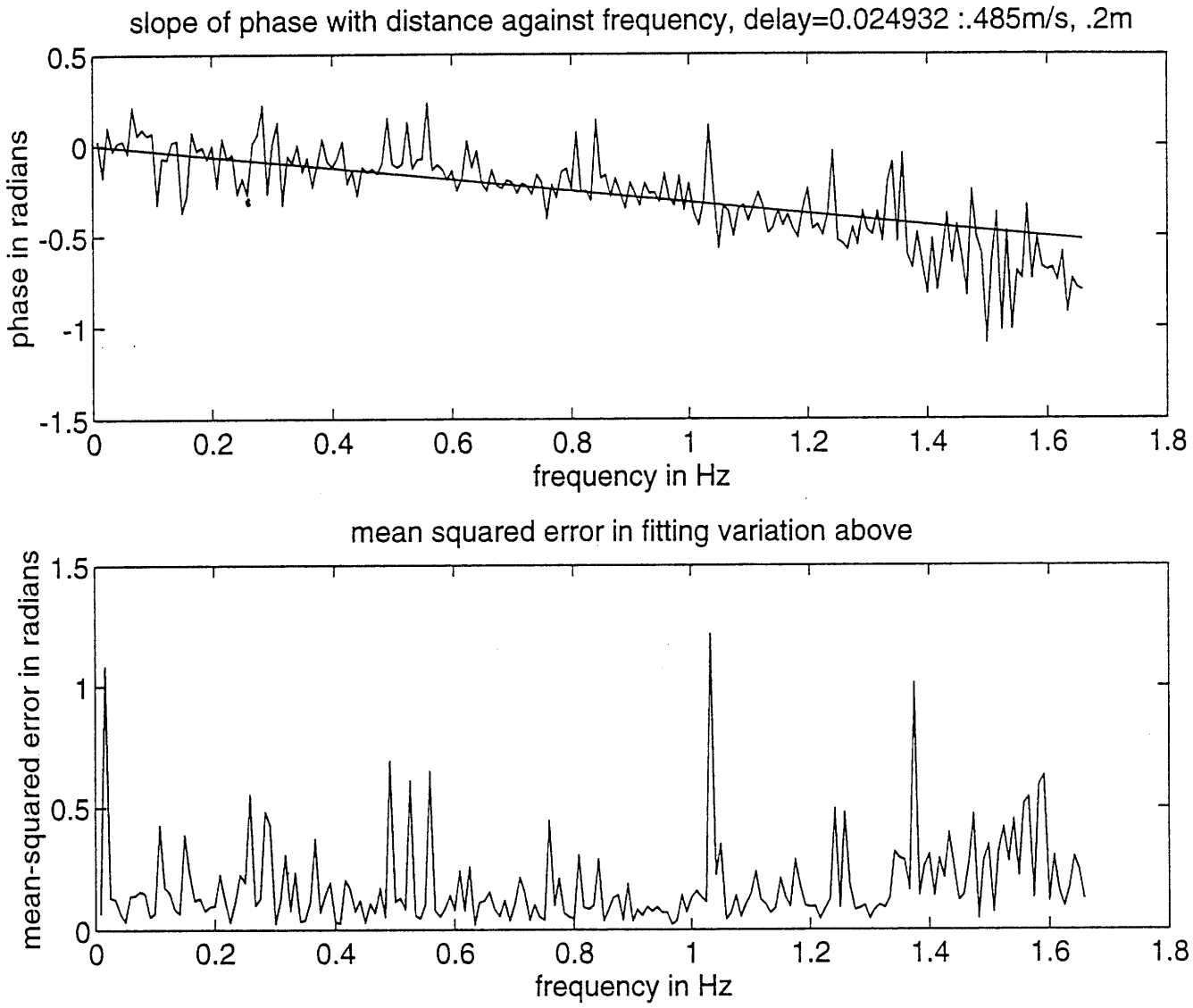

Figure 6-19: Transfer function angle slope against frequency: .485 m/s and .2m

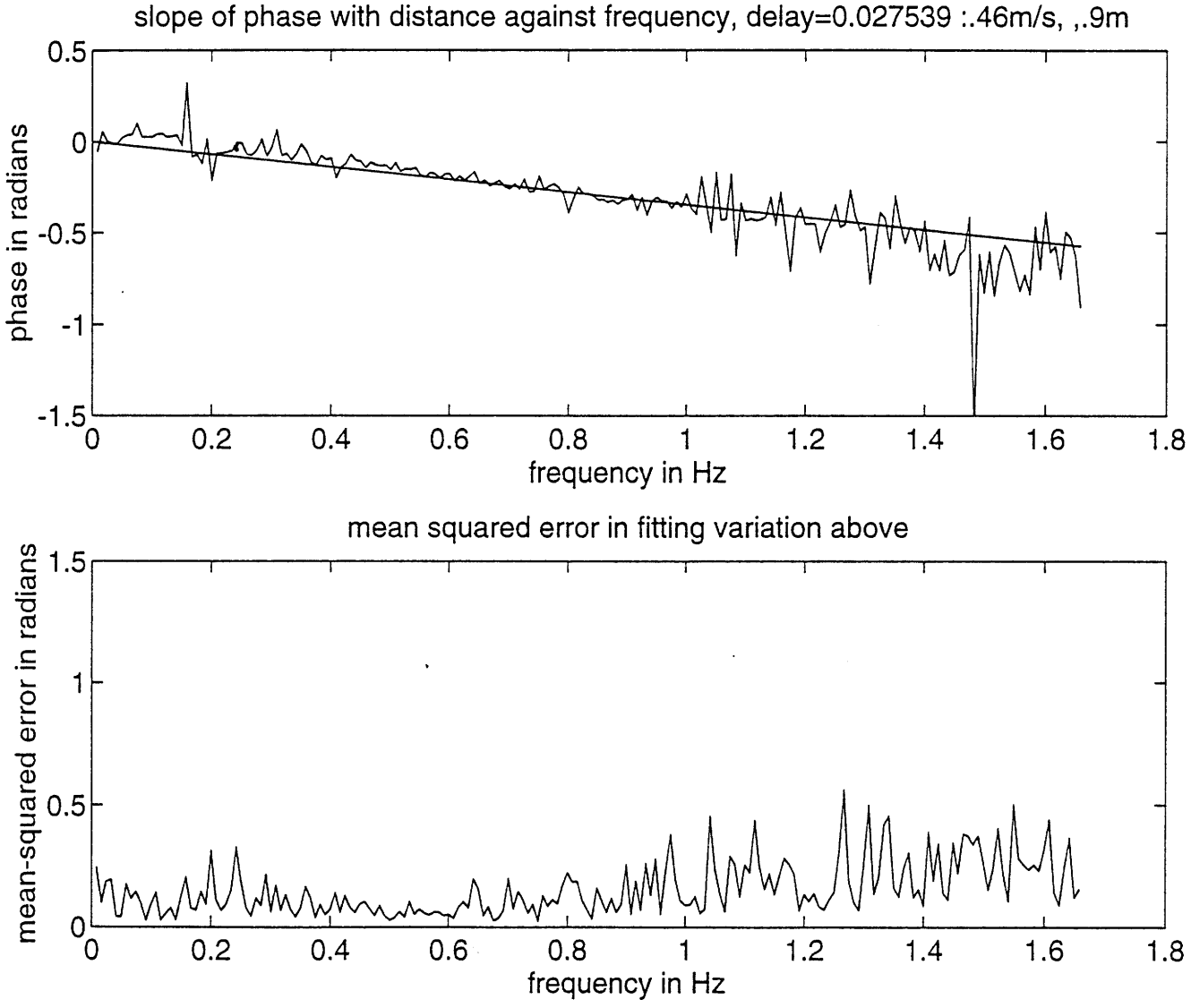

Figure 6-20: Transfer function angle slope against frequency: .46 m/s and .9m

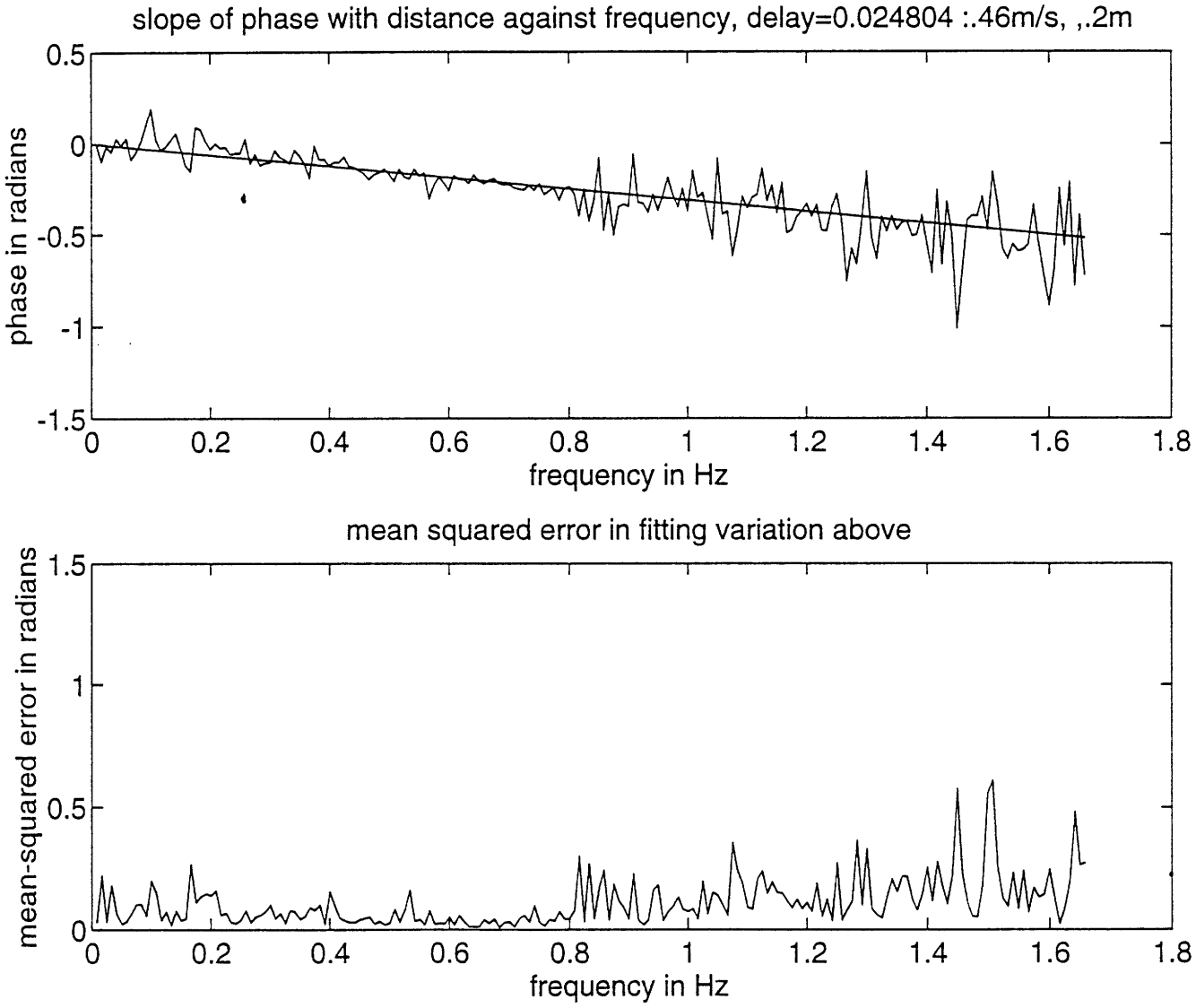

Figure 6-21: Transfer function angle slope against frequency: .46 m/s and .2m

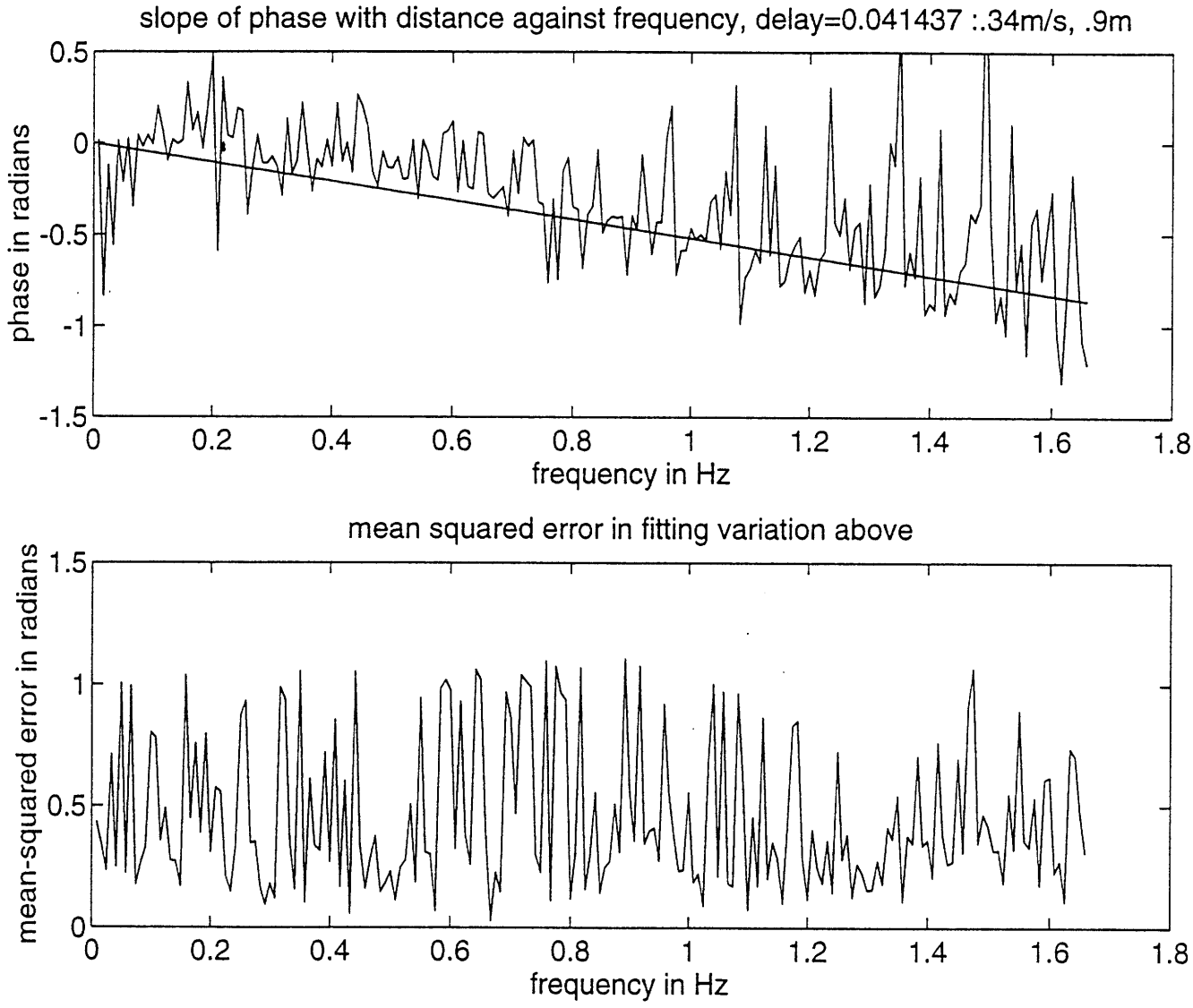

Figure 6-22: Transfer function angle slope against frequency: .34 m/s and .9m

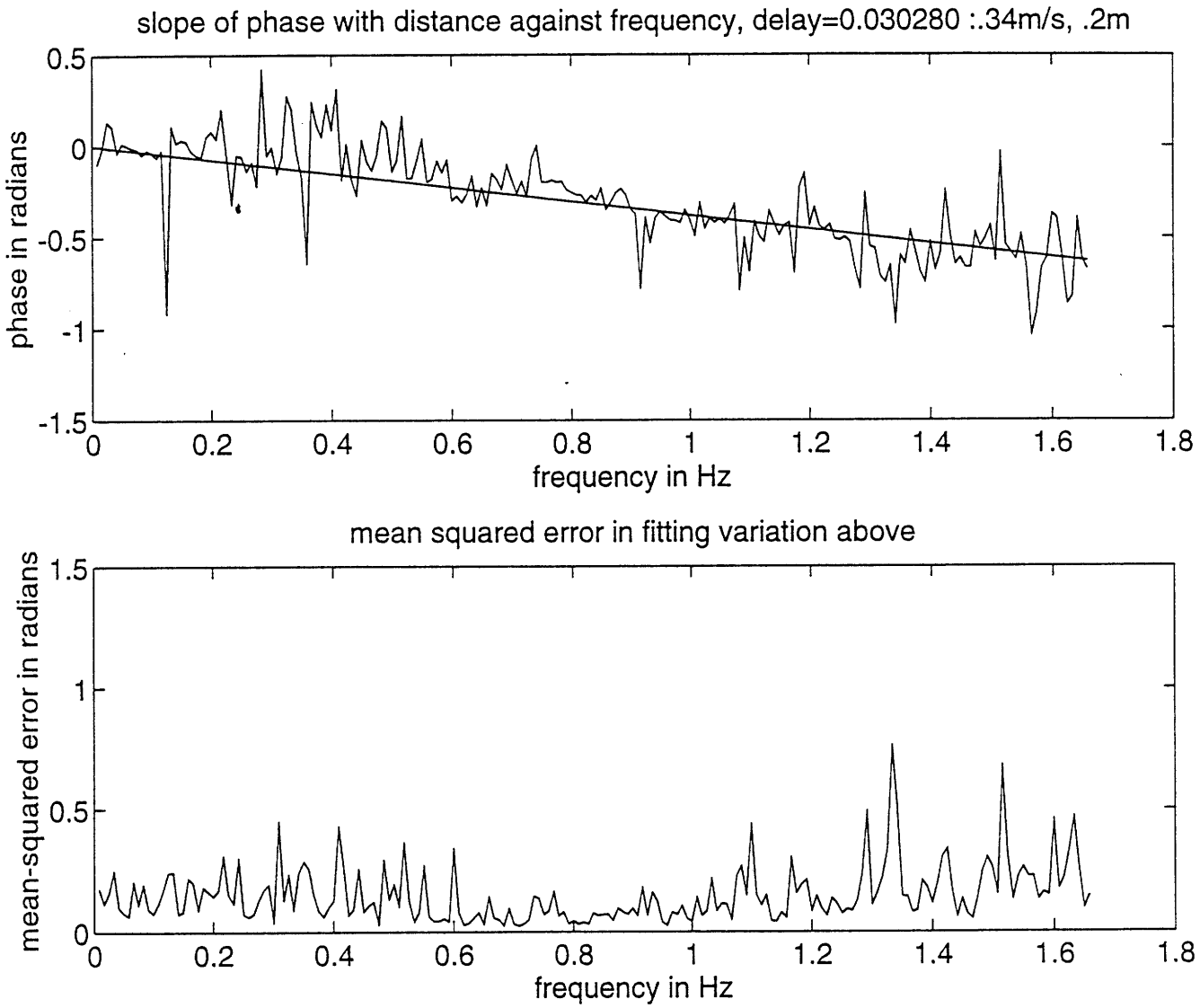

Figure 6-23: Transfer function angle slope against frequency: .34 m/s and .2m

Chapter 7

Conclusions and Recommendations

The experiment displayed the two main traits expected from the instability:

- all frequencies convected downstream at the same rate.
- a certain narrow band of frequencies became increasingly unstable at higher water-tunnel velocities

Thus we were able to create an infinite dimensional instability of uncountable dimension and were able to model it with a finite dimensional model.

However, there were certain problems with the experiment that made it problematic for the study of the control of the instability.

- the transfer function from the airfoil to the shear layer appeared to be dominantly non-linear above a certain threshold frequency. This complicates the process of controlling the instability.
- the airfoil was unable to excite frequencies above this threshold frequency. this corresponds to certain frequencies that are uncontrollable. If the tunnel were driven at a velocity so that these frequencies were unstable, the system would not be stabilizable.

- at higher velocities, the oil had a tendency of getting carried by the water flowing over it. This not only resulted in a loss in the expensive oil but the oil would corrode parts of the tunnel that were not covered with a protective lining.

Although the tunnel did show the desired traits, the problems listed above make the experiment impractical. If the experiment is to be continued, a different combination of fluids should be used. An alternative method of actuation that has no non-linearity should also be considered.

Bibliography

[Roberts and Sanders] G.E. Roberts and H Kaufmann *Table of Laplace Transforms* W.B. Sanders Company

[Weigl, 93] H. Weigl, *Personal conversations* 1993

[Paduano, 92] J.D. Paduano, *Active Control of Rotating Stall in Axial Compressors* MIT GTL Report no.208, March 1992.

[Banks] Banks *A state space approach to infinite dimensional systems*

[Math Works Inc.] The Math Works Inc. *Control Toolbox Users Guide*

[Van de Vegte, 90] John Van de Vegte *Feedback Control Systems*, Prentice-Hall Inc.,1990

[Kirk, 70] Donald E. Kirk *Optimal Control Theory*, Prentice-Hall Inc.,1970

[Chandrasekhar, 68] Chandrasekhar *Hydrodynamic and Hydromagnetic Stability*, Oxford at Clarendon Press, 1968

[McCune] James E. McCune *16.20 Class notes for Fluid Mechanics* Massachusetts Institute of Technology

[McCune, 88] James E. McCune *Unsteady Wing Theory - The Karman/Sears Legacy* AIAA-88-3540 AIAA 1st Natianal

fluid Dynamics Congress July 25-28, 1988, Cincinanati, Ohio

[Levine, 70] William S. Levine and Michael Athans, *On the Determination of the Optimal Constant Output Feedback Gains for Linear Multivariable Systems* IEEE Transactions on Automatic Control, Vol AC-15, NO1, February 1970